JOURNAL OF GUIDANCE, CONTROL, AND DYNAMICS
Vol. 34, No. 4, July–August 2011

Conflict Resolution in Converging Air Traffic Using Trajectory Patterns

Alfonso Valenzuela* and Damián Rivas†
Universidad de Sevilla, 41092 Sevilla, Spain

DOI: 10.2514/1.50751

A method for conflict detection and resolution based on the parameterization of the aircraft intents is presented. The method is also based on the use of predefined trajectory patterns, which are in fact flight intents; these patterns include standard airline procedures and air traffic control regulations. The conflict resolution problem is formulated as a parametric optimization problem subject to constraints; the optimality criterium is defined so that the deviation from the intended (preferred) trajectories in the lateral profile is minimized. The resolution trajectory patterns take into account changes of the nominal waypoints (vectoring) and changes of the aircraft speeds. The method is applied to the case of multiple conflicts among commercial transport aircraft in converging traffic in the terminal area; different scenarios are considered, which include locked aircraft, that is, aircraft whose trajectories are known and fixed. The conflict detection and resolution algorithm relies on a kinetic trajectory predictor (nonlinear point-mass model with variable mass), which is accurate, flexible, and transparent, and provides the high-fidelity prediction required in the analysis of the demanding terminal area traffic. The cost of the global conflict resolution process is assessed, in terms of extra distance traveled, extra flight time, and extra fuel consumed for each aircraft.

Nomenclature

a	=	speed of sound
C_C	=	specific fuel consumption coefficient
C_D	=	drag coefficient
C_L	=	lift coefficient
C_T	=	thrust coefficient
c	=	specific fuel consumption
D	=	drag
d	=	distance
d_{ij}	=	horizontal distance between aircraft i and j
d_s	=	horizontal separation minimum
$\mathbf{F}$	=	state equations
f	=	cost function
$\mathbf{G}$	=	flight constraint equations
g	=	gravity acceleration
$\mathbf{g}$	=	equality constraints
h	=	altitude
h_{ij}	=	vertical distance between aircraft i and j
h_s	=	vertical separation minimum
$\mathbf{h}$	=	inequality constraints
L	=	lift
M	=	Mach number
m	=	aircraft mass
m_F	=	fuel mass
n	=	number of unlocked aircraft
n_l	=	number of locked aircraft
p	=	pressure
R	=	turn radius
R_a	=	air gas constant
R_E	=	Earth radius
r	=	horizontal distance
S	=	wing area
T	=	thrust
t	=	time
t_f	=	flight time
$\mathbf{u}$	=	control vector
V	=	aerodynamic speed
$\mathbf{x}$	=	parameter vector
$\mathbf{y}$	=	state vector
γ	=	flight-path angle
δ	=	pressure ratio
Θ	=	temperature
θ	=	temperature ratio
κ	=	ratio of specific heats
λ	=	geodetic longitude
μ	=	bank angle
ρ	=	density
φ	=	geodetic latitude
χ	=	heading angle

Subscripts

A	=	given value
AP	=	approach
c	=	cruise
d	=	descent
SL	=	sea level (Instrument Standard Atmosphere model)

I. Introduction

THE need for increasing automation in the future air traffic management (ATM) system (proposed by NextGen and SESAR) makes it necessary to develop advanced automation tools to detect traffic conflicts and assist in their resolution. In the literature one can find different approaches to model the conflict detection and resolution (CDR) problem. Menon et al. [1] parameterize the actual trajectories in terms of 4-D (space and time) trajectory waypoints, and formulate an optimization problem; the trajectories are approximated by piecewise-linear paths. Frazzoli et al. [2] formulate the conflict resolution (CR) problem as a nonconvex quadratic programming problem, which is approximated by convex semidefinite programming. Hu et al. [3] formulate an optimal CR problem by defining an energy cost function for the joint maneuver, which must

Presented as Paper 2009-7022 at the 9th AIAA Aviation Technology, Integration, and Operations Conference and Aircraft Noise and Emissions Reduction Symposium, Hilton Head, SC, 21–23 September 2009; received 14 May 2010; revision received 1 December 2010; accepted for publication 31 January 2011.

*Assistant Professor, Department of Aerospace Engineering, Escuela Superior de Ingenieros; avalenzuela@us.es. Member AIAA.

†Professor, Department of Aerospace Engineering, Escuela Superior de Ingenieros; drivas@us.es. Member AIAA.

be conflict free; in the multiple-aircraft case, the original constrained optimization problem is approximated by a finite-dimensional convex optimization problem with linear constraints. Clements [4] formulates an optimal control problem, and computes optimal resolution maneuvers for conflicts between two aircraft; the avoidance maneuvers are flown at constant speed. Paielli [5] presents an iterative algorithm that searches for a combination of speed and heading maneuvers that resolves the conflict; the algorithm is applied to the case of conflicts between two aircraft. Raghunathan et al. [6] also formulate an optimal control problem, which is discretized into a nonlinear programming problem; they address the issue of flyability of the generated trajectories. Vivona et al. [7] use a genetic algorithm, as part of the CR method, to select and optimize a resolution maneuver from a set of predefined maneuver patterns. Bilimoria and Lee [8] consider the CR problem with the additional constraint of a fixed arrival time at a downstream waypoint; the resolution approach is divided into two general maneuvers: avoidance and recovery. All these works analyze enroute conflicts; Menon et al. [1] and Hu et al. [3] consider altitude changes in the resolution of the conflicts, whereas the rest of the works cited solve horizontal problems. Isaacson and Robinson [9] present a knowledge-based CR algorithm for terminal areas, used in center-TRACON automation system (CTAS) tools, which models the resolution tactics used by controllers. Other CDR modeling methods can be found in the review performed by Kuchar and Yang [10].

In this work, we present a CDR method based on the parameterization of the aircraft intents. To that end, we consider predefined *trajectory patterns*, which are in fact *flight intents*, that model the aircraft trajectories actually flown. The method is applied to the case of converging traffic in a terminal area (TMA), so that the trajectory patterns consider the flight segments usually flown by transport aircraft in cruise and descent (e.g., idle descents), and include standard airline procedures (e.g., standard arrival STAR) and air traffic control regulations (e.g., speed limitation below 10,000 ft). In this work the nominal (intended) trajectories and the operator preferences are supposed known.

Predefined trajectory patterns to treat CDR problems have been used by different authors. Vilaplana [11] defines a lateral shift maneuver, as a sequence of straight lines connected by inside turns, to solve enroute conflicts. Vivona et al. [7] consider a CR algorithm based on predefined maneuver patterns (lateral offset, direct intercept path, path stretch, waypoint migration, and cruise step climb/descent), designed to execute different types of user-accepted path modification. Coppenbarger et al. [12] describe the Enroute Descent Advisor (EDA), a CTAS tool that solves the meet-time problem, where the cruise and descent speeds are used as parameters, and a simple "dog-leg" maneuver is considered for lateral routing (path stretching to absorb large delays). In other contexts, Gill and Maddock [13] use predefined strategies to meet time and altitude constraints within the PHARE programme, Slattery and Zhao [14] use predefined profile types (fast, nominal, and slow) to synthesize cruise-descent trajectories for air traffic automation, Jackson et al. [15] consider nominal descent profiles (formed by five segments) to study the sensitivity of trajectory prediction, and Barrer [16] considers predefined patterns called path objects as a means to standardize flight procedures.

In this work, the trajectory patterns defined for the case of converging traffic are described in terms of a small number of free parameters, both from the vertical profile (e.g., speeds) and from the lateral profile (e.g., waypoint coordinates). Note that a trajectory is completely determined if the values of these parameters are fixed. The CR problem is then formulated as a parametric optimization problem subject to constraints; the CR algorithm yields the values of the parameters, for all aircraft involved, that solve the conflicts, while minimizing the deviation from the intended trajectories in the lateral profile (this is the chosen performance index). The resolution trajectory patterns take into account changes of the nominal waypoints (vectoring) and changes of the aircraft speeds. The resolution strategy is composed of two phases: one in which a first valid solution is found by means of a random search, and another in which this first valid solution is optimized (that is, another valid solution with smaller cost is found). The conflict detection (CD) algorithm considers both horizontal and vertical separation standards.

The CDR algorithm must rely on a trajectory predictor, which can be of different levels of complexity. On one side, one has the case of kinematic trajectory modeling (see, for instance, Bilimoria [17]), in which speed and heading changes are modeled as instantaneous maneuvers. On the other side, one has the general case of nonlinear point-mass kinetic trajectory modeling (see, for instance, Menon et al. [1]), in which the maneuver dynamics is taken into account. Paielli [5], however, presents an intermediate approach, in which speed and heading changes are modeled by simple maneuvers; this model improves over those in which speed and heading changes are instantaneous, but lacks the accuracy of general nonlinear point-mass dynamic models.

The CDR problem in converging traffic in the terminal area requires the use of a general nonlinear point-mass kinetic model, so that one has the accuracy required by this demanding traffic scenario. This is the case considered in this work. We present a dynamic nonlinear trajectory predictor in which realistic aerodynamic and engine models (based on BADA 3.6) are used, such that the dynamic flight paths are handled with the required precision. A simplified version with instantaneous heading changes is presented in Valenzuela and Rivas [18].

According to the taxonomy given by Kuchar and Yang [10] the method presented in this paper can be categorized as: three-dimensional state information, nominal dynamic state propagation (without uncertainty), optimized conflict resolution, turns and speed change maneuvers, and global handling of the potential conflicts; it is also strategic and centralized, and considers multiple aircraft.

Bilimoria et al. [19] propose the use of three metrics to evaluate the performance of a CDR scheme: safety, efficiency, and stability. The method presented in this work is safe and stable, because it solves all the conflicts and is centralized and global, and its efficiency is established by assessing the cost of the global CR process, in terms of extra distance traveled, extra flight time, and extra fuel consumed for each aircraft.

As already mentioned, the CDR method is applied to the case of converging traffic in a TMA, and two different scenarios are considered. First, one in which all aircraft are unlocked, that is, their trajectories are subject to change in the resolution process; and a second one in which there are some unlocked aircraft and some locked aircraft, that is, aircraft whose trajectories are known and fixed. Unlocked aircraft can be in conflict both with the other unlocked and with the locked aircraft. The resolution of the problem requires that the unlocked aircraft be conflict free with all aircraft, both locked and unlocked. Results for the case of multiple conflicts among commercial transport aircraft in Madrid TMA are presented.

The outline of the paper is as follows: the trajectory patterns are defined in Sec. II, the CDR problem is formulated in Sec. III, the scenarios considered are described in Sec. IV, the results are presented in Sec. V, and some conclusions are drawn in Sec. VI; the trajectory computation solver is described in Appendix A, and the Earth and aircraft models used are described in Appendix B.

II. Trajectory Patterns

The CDR method presented in this work is based on the use of trajectory patterns, which are, in fact, flight intents that model both the vertical profile (altitude, speed, engine) and the lateral profile (route, turns); to define them, the operator preferences are supposed known. These trajectory patterns are described in terms of a small number of free parameters (this is important in the resolution process). Two types of trajectory patterns are considered: 1) nominal trajectory patterns, which model the aircraft intended trajectories, and 2) resolution trajectory patterns, which model the aircraft resolution trajectories. These are modifications of the nominal trajectory patterns assigned to the aircraft, which must be physically executable. Either one or both of the vertical and lateral profiles can be modified. The modifications may change the parameters defining some flight segments, may eliminate some segments, and may also add new segments. The resolution trajectory patterns take into

account changes of the nominal waypoints (vectoring) and changes of the aircraft speeds. Each aircraft can have a different resolution trajectory pattern assigned.

In this paper conflict detection and resolution in converging traffic within a TMA is analyzed. Hence, we consider resolution trajectories (flight intents) that model the cruise and descent phases.

A. Nominal Trajectory Patterns

In principle, each aircraft can have a different nominal trajectory pattern assigned, although in this work all aircraft have the same one, as follows (note that one could choose a different flight intent). *Lateral profile*: 1) defined by waypoints, and 2) turns at constant bank angle. *Vertical profile* (see Fig. 1): 1) constant Mach M_c, constant altitude h_c cruise, until the cruise speed reduction (CSR) point (this point is the beginning of the last segment of the cruise phase, which is a deceleration at cruise altitude that ends at the TOD point), 2) horizontal deceleration at cruise altitude, with idle engine rating, until the Mach of descent M_d is reached, from the CSR point to the TOD point, 3) Mach/calibrated air speed (CAS) descent (speeds M_d, CAS_d), with idle engine rating, until 10,000 ft, 4) horizontal deceleration at 10,000 ft, with idle engine rating, until 250 kt, 5) constant CAS descent (250 kt), with idle engine rating, until glide-path interception altitude h_{ILS}, 6) horizontal deceleration at glide-path interception altitude, with idle engine rating, until the approach speed $\mathrm{CAS}_{\mathrm{AP}}$ (lift devices for approach are deployed during this segment), 7) constant CAS $\mathrm{CAS}_{\mathrm{AP}}$, constant altitude h_{ILS} segment of length 0.5 nmi (landing gear and lift devices for landing are deployed during this segment), and 8) glide path segment at constant CAS $\mathrm{CAS}_{\mathrm{AP}}$ and constant path angle ($\gamma = -3^\circ$).

This vertical profile is quite similar to the flight profile used in the Experimental Flight Management System of the PHARE programme (see [13]).

Note that pull-ups or push-downs are not considered. The aircraft can enter the TMA while flying any of the above segments above 10,000 ft. The CSR point (and, as a consequence, the TOD point) is determined iteratively. Arrows in Fig. 1 indicate the stopping condition for the corresponding flight segment.

B. Resolution Trajectory Patterns

The resolution trajectory patterns are now modifications of the nominal trajectory pattern both in the lateral and vertical profiles. The modification in the lateral profile is as follows: all the waypoints of the nominal trajectory pattern in the TMA, except the TMA entry point, the initial fix approach (IAF), and those after the IAF, may be changed, keeping fixed the total number of waypoints (it has been decided not to change the lateral profile after the IAF). The modification in the vertical profile consists in introducing speed changes, in cruise and in descent above 10,000 ft (it has been decided not to change the speed profile below 10,000 ft); moreover, it has been decided not to introduce altitude changes.

Thus, in general, besides the coordinates of the modifiable waypoints (longitude and latitude), the parameters of the nominal trajectory pattern that can be modified are the following speeds: cruise Mach, descent Mach, and descent CAS; let M_c^*, M_d^*, CAS_d^* be the modified values.

Different patterns are considered depending on the flight phase (cruise, descent, and so forth) the aircraft is flying when it enters the TMA. These patterns are described next.

1. Pattern A

The aircraft enters the TMA while cruising (before reaching the CSR point), see Fig. 2. The parameters free to be changed and define the resolution trajectory in this case are the speeds M_c, M_d, CAS_d, and the coordinates of the modifiable waypoints λ_i, φ_i. The change in cruise speed requires a new flight segment: horizontal acceleration/deceleration at cruise altitude, from the nominal to the modified cruise Mach M_c^*, with maximum cruise/idle engine rating. To define the resolution trajectory the new CSR point must be calculated (by iteration), say CSR*, which in general is different from the CSR point of the nominal trajectory. The horizontal distance between the TMA entry point and the IAF can be larger or smaller than the one corresponding to the nominal trajectory, that is, the nominal route can be lengthened or shortened.

The changes in the speed profile parameters are subject to the following constraints:

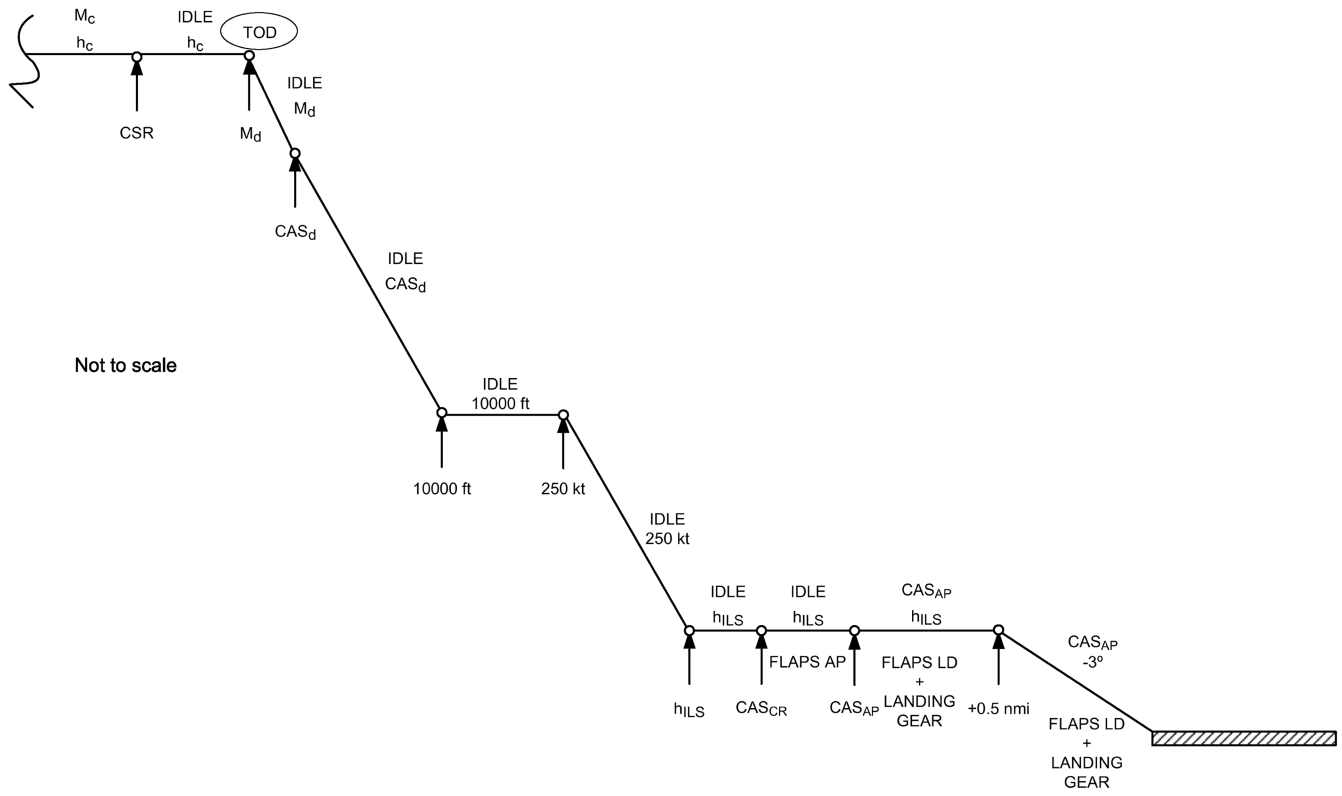

Fig. 1 Sketch of the nominal trajectory pattern (flight intent).

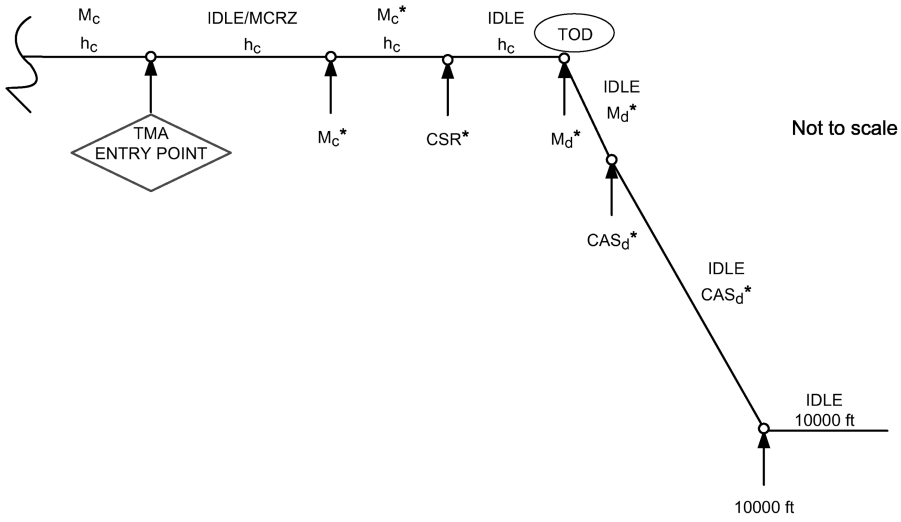

Fig. 2 Resolution trajectory pattern A.

1) They must be changed within some limits. We consider changes within $\pm 10\%$ of the nominal values:

$$|M_c^* - M_c| \leq 0.1 M_c \qquad |M_d^* - M_d| \leq 0.1 M_d$$
$$|\mathrm{CAS}_d^* - \mathrm{CAS}_d| \leq 0.1 \mathrm{CAS}_d \tag{1}$$

2) The descent Mach is always smaller than or equal to the cruise Mach:

$$M_d^* \leq M_c^* \tag{2}$$

3) The descent CAS is always larger than or equal to 250 kt:

$$\mathrm{CAS}_d^* \geq 250 \text{ kt} \tag{3}$$

4) The descent Mach and CAS must be such that the transition altitude h_{TR} is smaller than or equal to the cruise altitude and larger than or equal to 10,000 ft:

$$10,000 \text{ ft} \leq h_{\mathrm{TR}}(M_d^*, CAS_d^*) \leq h_c \tag{4}$$

The changes in the waypoints coordinates are subject to the constraint that they must be inside boxes centered on the nominal waypoints, that is:

$$|\lambda_i - \lambda_i^0| \leq 0.3 \text{ deg} \qquad |\varphi_i - \varphi_i^0| \leq 0.3 \text{ deg} \tag{5}$$

This constraint enforces that the resolution trajectory does not deviate too much from the preferred trajectory.

2. Pattern B

The aircraft enters the TMA flying the last cruise deceleration segment, between the CSR and the TOD points, see Fig. 3. The parameters free to be changed in this case are the descent speeds M_d, CAS_d, and the coordinates of the modifiable waypoints λ_i, φ_i. The cruise deceleration segment now ends when the new descent Mach M_d^* is reached. After the deceleration, a new flight segment is added: cruise altitude and constant Mach M_d^*, ending at the new TOD point, say TOD*, which must be determined iteratively.

The changes in the speed profile parameters are subject to the following constraints:

1) They must be changed within $\pm 10\%$ of the nominal values:

$$|M_d^* - M_d| \leq 0.1 M_d \qquad |\mathrm{CAS}_d^* - \mathrm{CAS}_d| \leq 0.1 \mathrm{CAS}_d \tag{6}$$

2) The descent Mach is always smaller than or equal to the Mach at the TMA entry point M_{TMA}:

$$M_d^* \leq M_{\mathrm{TMA}} \tag{7}$$

3) The descent CAS is always larger than or equal to 250 kt, as given by Eq. (3).

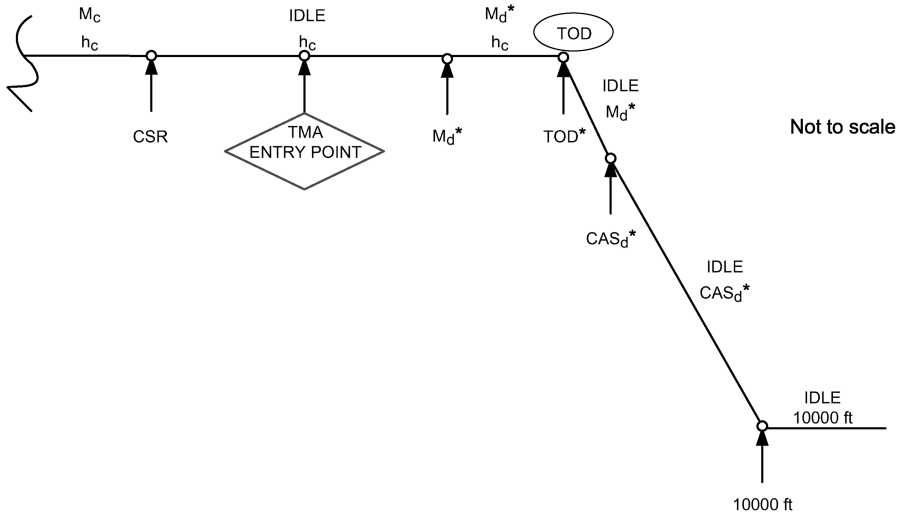

Fig. 3 Resolution trajectory pattern B.

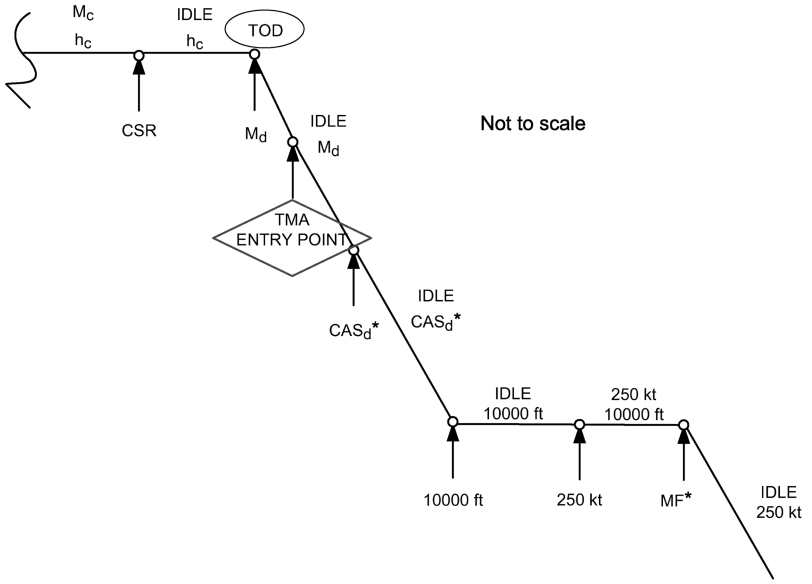

Fig. 4 Resolution trajectory pattern C.

4) The descent Mach and CAS must be such that the transition altitude h_{TR} is smaller than or equal to the cruise altitude and larger than or equal to 10,000 ft, as given by Eq. (4).

As in pattern A, the changes in waypoints coordinates must be inside boxes centered on the nominal waypoints; the constraints are given by Eq. (5).

3. Pattern C

The aircraft enters the TMA flying the constant-Mach descent segment, see Fig. 4. In this case, the parameters free to be changed and define the resolution trajectory are the CAS descent speed CAS_d and the coordinates of the modifiable waypoints λ_i, φ_i. The constant-Mach descent segment is flown with the nominal Mach M_d, ending now when the new descent CAS CAS_d^* is reached. After the deceleration at 10,000 ft, a new segment is added: constant CAS (250 kt) at 10,000 ft, ending at a metering fix MF* that must be determined iteratively.

The changes in the speed profile parameters are subject to the following constraints:

1) They must be changed within $\pm 10\%$ of the nominal values:

$$|\mathrm{CAS}_d^* - \mathrm{CAS}_d| \leq 0.1\mathrm{CAS}_d \tag{8}$$

2) The descent CAS is larger than or equal to 250 kt, as given by Eq. (3).

3) The descent Mach and CAS must be such that the transition altitude (h_{TR}) is smaller than or equal to the altitude of the TMA entry point (h_{TMA}) and larger than or equal to 10,000 ft:

$$10,000 \text{ ft} \leq h_{\mathrm{TR}}(M_d, \mathrm{CAS}_d^*) \leq h_{\mathrm{TMA}} \tag{9}$$

Again, the changes in waypoints coordinates must be inside boxes centered on the nominal waypoints; the constraints are given by Eq. (5).

4. Pattern D

The aircraft enters the TMA flying the constant-CAS descent segment, see Fig. 5. Now, the parameters free to be changed and define the resolution trajectory are just the coordinates of the modifiable waypoints λ_i, φ_i. The constant-CAS descent segment is

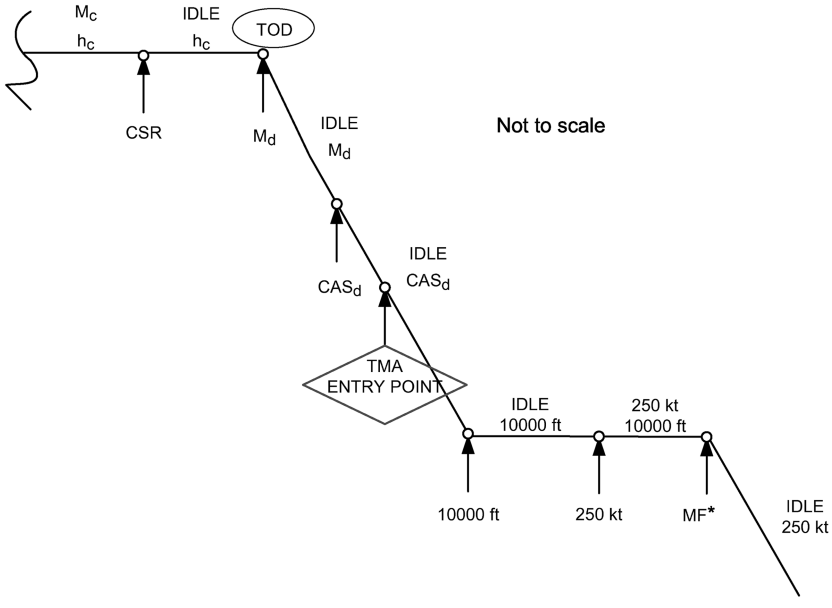

Fig. 5 Resolution trajectory pattern D.

flown with the nominal CAS CAS_d. After the deceleration at 10,000 ft, a new segment is added: constant CAS (250 kt) at 10,000 ft, ending at a metering fix MF* that must be determined iteratively.

The changes in the coordinates of the modifiable waypoints are subject to the constraint that, as in previous cases, they must be inside boxes centered on the nominal waypoints, that is, as given by Eq. (5).

III. CDR Problem Formulation

In general, the TMA scenario is defined by a limited region of airspace where there are a set of aircraft whose nominal trajectories (the intended trajectories) are in conflict. Some of these aircraft can be locked, that is, their trajectories are known and fixed; the rest of the aircraft are unlocked, that is, their trajectories can be modified during the conflict resolution process. Locked aircraft are conflict free among them, whereas unlocked aircraft can be in conflict with both the locked and the other unlocked aircraft. The resolution of the problem requires that the unlocked aircraft be conflict free with all aircraft (locked and unlocked). Let n be the number of unlocked aircraft and n_l the number of locked aircraft.

The resolution process is centralized, that is, there exists a *control station* that determines the resolution trajectories; all the aircraft fly the resolution trajectories proposed by the control station. The process is also strategic, that is, the intended trajectories are known to the control station well in advance, to carry out the resolution process before the aircraft enter the TMA.

In this work uncertainties are not considered.

A. Conflict Detection

The CD process evaluates the separation between any pair of aircraft during their flights, by comparing the separation between them with the separation minima applicable. In this work distance separation is considered, hence the CD algorithm measures distance between pairs of aircraft.

The input is the state vector of all aircraft, $\mathbf{y}_i(t)$, $i = 1, \ldots, n + n_l$, and the output are the horizontal and vertical distances between all pairs of aircraft, except the pairs of locked aircraft, $d_{ij}(t_k)$ and $h_{ij}(t_k)$, $i = 1, \ldots, n$, $j = 1, \ldots, n + n_l$, $i \neq j$, respectively. The distances are measured at discrete times $t_k = t_0 + k\Delta t$, $k = 1, 2, 3, \ldots$, during the time they both are in the TMA (when the state variables are not known at time t_k, linear interpolation is used). The minimum horizontal and vertical distances, $(d_{ij})_{\min}$ and $(h_{ij})_{\min}$, are computed and compared with the separation minima, d_s and h_s, that correspond to each pair of aircraft; a conflict between aircraft i and j is detected when the following condition holds

$$\max\left(\frac{(d_{ij})_{\min}}{d_s}, \frac{(h_{ij})_{\min}}{h_s}\right) < 1 \tag{10}$$

(this definition of conflict is taken from [20]).

This way of detecting the conflicts allows one to consider altogether all the violations of the separation minima that can occur between two aircraft trajectories along the whole flight, so that in case that a proposed trajectory modification solves one loss of separation but leads to new losses, the aircraft trajectory will be still in conflict and the proposed modification will not be accepted.

The horizontal distance between two aircraft is measured along a great circle (minimum distance) on the Earth surface, which is given by

$$d_{ij} = R_E \cos^{-1}[\sin\varphi_i \sin\varphi_j + \cos\varphi_i \cos\varphi_j \cos(\lambda_j - \lambda_i)] \tag{11}$$

where (λ_i, φ_i) and (λ_j, φ_j) are the geodetic coordinates of the aircraft horizontal positions and R_E is the Earth radius. The vertical distance is just

$$h_{ij} = |h_i - h_j| \tag{12}$$

Other CD algorithms with more complex logics can be found in [21,22], developed for CTAS and PHARE, respectively.

B. Conflict Resolution

The CR process generates a set of trajectories that resolves the potential conflicts detected by the CD process (i.e., a set of trajectories that meet the separation criteria), while optimizing a given performance index.

In general, each unlocked aircraft i has assigned a resolution trajectory pattern. The corresponding resolution trajectory is then described in terms of a set of parameters $\mathbf{x}_i$ (waypoints coordinates and speeds in our case, although one could also have altitudes, times, distances, and so forth). The set of trajectories corresponding to the n unlocked aircraft is collected in a vector of parameters $\mathbf{x}$:

$$\mathbf{x} = [\,\mathbf{x}_1^T \quad \ldots \quad \mathbf{x}_i^T \quad \ldots \quad \mathbf{x}_n^T\,]^T \tag{13}$$

so that the CR problem is formulated as a constrained parametric optimization problem, including equality and inequality constraints, as follows:

$$\begin{aligned} &\text{minimize the cost function } f(\mathbf{x}) \\ &\text{subject to the constraints } \mathbf{g}(\mathbf{x}) = \mathbf{0} \qquad \mathbf{h}(\mathbf{x}) \leq \mathbf{0} \end{aligned} \tag{14}$$

1. Parameters

The parameters considered in the resolution process depend on the resolution trajectory pattern under consideration (namely, A, B, C, or D), as described above in Sec. II.B.

2. Cost Function

In principle, the optimality criterium defining the cost function (performance index) can be the minimization (or maximization) of any property or combination of properties that can be derived from the resolution trajectories (for example, any combination of fuel and time costs, deviation from the nominal trajectories, etc.). In this work the optimality criterium is defined to minimize the deviation from the nominal trajectories in the lateral profile. The objective function selected is:

$$f(\mathbf{x}) = \sqrt{\sum_{i=1}^{m}[(\lambda_i - \lambda_i^0)^2 + (\varphi_i - \varphi_i^0)^2]} \tag{15}$$

where $(\lambda_i^0, \varphi_i^0)$ are the nominal location of the waypoints and m is the total number of waypoints that can be changed.

3. Constraints

The constraints considered in this paper can be classified as follows:

1) Traffic constraints: the resolution trajectories have to be conflict free ($(d_{ij})_{\min} \geq d_s$ or $(h_{ij})_{\min} \geq h_s$), among themselves and with the fixed trajectories of the locked aircraft; all the waypoints must be inside the TMA; and the resolution trajectories have to end in the runway threshold.

2) Method constraints: constraints defined by the trajectory patterns (see Sec. II.B), which depend on the resolution trajectory pattern under consideration (namely, A, B, C or D).

3) Aircraft constraints: all the speeds have to be inside the operational envelopes.

These constraints can be also classified as *individual* constraints and *dual* constraints. Individual constraints affect to only one trajectory $\mathbf{x}_i$ (e.g., aircraft constraints). Dual constraints link pairs of trajectories $\mathbf{x}_i$ and $\mathbf{x}_j$ (e.g., loss of separation between unlocked aircraft). As it is will be shown below, this classification is important in the resolution strategy.

4. Resolution Strategy

In this work the resolution process is divided into two phases:

Random Search of a First Valid Solution: The objective is to find a set of resolution trajectories that solve the conflicts, although the trajectories found may not be too efficient (that is, to find a set of parameters $\mathbf{x}$ that satisfy the constraints). This phase is carried out following the iterative procedure described next.

First, a resolution trajectory is randomly generated for each unlocked aircraft, that is, for each unlocked aircraft a vector $\mathbf{x}_i$ that meets the individual constraints is randomly generated (in the random search, a uniform distribution is used). Thus, at iteration p, p randomly generated resolution trajectories and 1 nominal trajectory are available for each aircraft, that is, $p+1$ trajectories that meet the individual constraints. This means that, for the n aircraft, one has $(p+1)^n$ possible combinations of trajectories, formed by choosing one trajectory from the $p+1$ that correspond to each aircraft, so that each combination is a candidate solution of the conflict resolution process.

Next, for each of the $(p+1)^n$ trajectory combinations, the dual constraints are checked. In fact, because at iteration $p-1$ many of these combinations were checked, only those combinations that have at least one of the new resolution trajectories generated at this iteration are checked (in total, $(p+1)^n - p^n$ combinations).

If one or more combinations meet all the constraints, then the lowest-cost combination is chosen as first valid solution. If, on the other hand, no combination meets the constraints, then a new iteration is performed.

The objective of this combinatorial approach is to reduce the number of trajectory computations, which is the most time-consuming step in the whole resolution process.

Note that, in this first phase, in the process of finding a feasible initial point, one could have also considered other more advanced algorithms such as penalty methods (see [23]). In our approach, we have combined the simple random algorithm with the combinatorial approach just described to make the overall method efficient and suitable to our problem, in the sense of performing a small number of trajectory computations. Indeed, it is shown below that, with the computation of only 9 trajectories for each aircraft, a total of 10,000 combinations of trajectories are analyzed in Scenario 1 (Sec. V.A.2), and with the computation of 16 trajectories for each aircraft, a total of 83,521 combinations are analyzed in Scenario 2 (Sec. V.B.2).

Improvement of the First Valid Solution: The objective now is to improve the first valid solution found in the first phase, that is, to find another valid solution with smaller cost. This second phase is carried out by solving the parametric optimization problem (14), using that first valid solution as the starting point. Note that the landing sequence of the first valid solution is not imposed as a constraint, so that it can change during the optimization process.

In this work, both the cost function and the constraints are nonlinear, hence the optimization problem is a nonlinear programming problem. The optimization solver used in the simulations is MATLAB's *fmincon*, a SQP (sequential quadratic programming) method, which is widely considered as one of the most effective general methods for solving nonlinear programming problems (see [24]). The *fmincon* solver implements an active-set algorithm to manage the inequality constraints, which again is one of the most popular approaches to solving inequality quadratic problems (see [24]), and uses a BFGS (Broyden–Fletcher–Goldfarb–Shanno) updating formula to approximate the Hessians (preferable over other methods, according to [25]).

C. Trajectory Computation

The CDR process relies on a trajectory computation tool that solves the aircraft equations of motion for given *flight constraints* (each flight segment is defined by a set of three flight constraints). The formulation is then defined by a system of differential algebraic equations (DAE), of the following form:

$$\dot{\mathbf{y}} = \mathbf{F}(\mathbf{y}, \mathbf{u}, t) \qquad \mathbf{G}(\mathbf{y}, \mathbf{u}, t) = 0 \tag{16}$$

where $\mathbf{y}$ is the state vector and $\mathbf{u}$ the control vector.

In this paper the model adopted to describe the aircraft motion is that of a point mass with three degrees of freedom, commonly used for trajectory prediction (see [14]); the equations then describe the motion of the aircraft center of mass, considered as a mass-varying body. The scalar equations of motion are formulated based on the following general assumptions: spherical, nonrotating Earth; rigid and symmetric aircraft; symmetric flight; and thrust parallel to the aircraft aerodynamic velocity. These assumptions are appropriate for subsonic, transport aircraft. An additional assumption is that there is no wind. Hence, the scalar equations of motion are:

$$\begin{aligned}
m\frac{\mathrm{d}V}{\mathrm{d}t} &= T - D(V,h,L) - mg\sin\gamma \\
mV\cos\gamma\frac{\mathrm{d}\chi}{\mathrm{d}t} &= L\sin\mu \\
mV\frac{\mathrm{d}\gamma}{\mathrm{d}t} &= L\cos\mu - mg\cos\gamma \\
\frac{\mathrm{d}m}{\mathrm{d}t} &= -c(V,h)T \\
(R_E+h)\frac{\mathrm{d}\varphi}{\mathrm{d}t} &= V\cos\gamma\cos\chi \\
(R_E+h)\cos\varphi\frac{\mathrm{d}\lambda}{\mathrm{d}t} &= V\cos\gamma\sin\chi \\
\frac{\mathrm{d}h}{\mathrm{d}t} &= V\sin\gamma
\end{aligned} \tag{17}$$

In this formulation one has seven state variables $(V, \chi, \gamma, m, \varphi, \lambda, h)$ and three control variables (T, L, μ).

To complete the DAE system, three flight constraints must be specified for each flight segment; in general, they have the form

$$G_i(V,\gamma,\chi,m,\varphi,\lambda,h,T,L,\mu,t) = 0, \qquad i = 1,2,3 \tag{18}$$

The resolution of the DAE system for each flight segment is based on its reduction to a system of ordinary differential equations (ODE) through the explicit utilization of the flight constraints; this can be done in all cases considered in this paper. The ODE system is then solved using MATLAB's *ode45*. The resolution process for the different flight segments considered in this paper is described in Appendix A.

Additionally, to solve the problem, some supplementary models are needed: Earth, aerodynamic, and propulsion models. In this paper the aircraft models are based on BADA 3.6 [26], the atmosphere model is ISA, and the Earth has constant gravity. They are described in more detail in Appendix B.

1. Flight Constraints

The imposed flight constraints must be compatible and physically meaningful, that is, they must close the mathematical problem. In [27] one can find a complete description of the different flight constraints that are meaningful in the ATM context (they call *instructions* the flight constraints, and *operation* the set formed by them).

In this paper all the flight segments considered are defined by the following types of flight constraints:

1) Constant γ, χ, h, μ: In these cases, the constraint sets the value of a state variable (path angle, heading angle, altitude) or a control variable (bank angle).

2) Given T_{RATE}: In cases where the engine rating is given, this constraint defines the thrust law: $T_{\mathrm{MCRZ}}(M,h)$ for maximum cruise or $T_{\mathrm{IDLE}}(M,h)$ for idle (the maximum cruise rating is used to accelerate).

3) Constant M. When the Mach number is constant, say M_A, this constraint is equivalent to

$$V = M_A\sqrt{\kappa R_a \Theta(h)} \tag{19}$$

that is, one has a known speed law $V(h)$, say $V = V_M(h)$ (κ and R_a are given in Appendix B).

4) Constant CAS: When the CAS is constant, say CAS_A, this constraint is equivalent to (see [28])

$$V = \sqrt{\frac{2}{k}R_a\Theta(h)\left[\left(1+\frac{p_{\mathrm{SL}}}{p(h)}\left[\left(1+\frac{k}{2}\frac{\rho_{\mathrm{SL}}}{p_{\mathrm{SL}}}\mathrm{CAS}_A^2\right)^{1/k}-1\right]\right)^k - 1\right]} \tag{20}$$

where $k = (\kappa-1)/\kappa$; that is, one has another known speed law $V(h)$, say $V = V_C(h)$.

2. Initial and Stopping Conditions

The computation of each flight segment starts with the corresponding initial conditions and ends when the appropriate stopping condition is reached (for instance, reaching a given altitude, or a given Mach). The initial conditions must be compatible with the flight constraints.

The initial conditions of the first segment are given data. For any other segment, the initial conditions are the final conditions of the previous segment, except for the path angle, variable that may be discontinuous since pull-ups or push-downs are not considered (see Sec. II.A). In descent segments, the initial value of γ is estimated using an approximation of the normal-force equation obtained after neglecting the term $\frac{\mathrm{d}\gamma}{\mathrm{d}t}$.

A total of four stopping conditions considered in this paper are analyzed now:

1) Reach a given Mach or CAS. In this case, from the computed values of V and h, the corresponding value of Mach or CAS, defined by Eqs. (19) and (20), must be monitored during the integration, to determine when the event is reached.

2) Reach a given altitude. Altitude is a computed variable that must be monitored.

3) Reach a given heading. Heading angle is a computed variable that must be monitored.

4) Reach a given horizontal distance (along the Earth's surface). The horizontal distance traveled by the aircraft along the surface of the Earth r is defined by

$$\frac{\mathrm{d}r}{\mathrm{d}t} = \frac{R_E}{R_E + h} V \cos\gamma \tag{21}$$

Thus, this equation must be integrated along the trajectory, and the variable r must be monitored.

3. Turns

In this work we consider inside turns at constant bank angle ($\mu = \mu_A$). Thus, the turning segment is defined by the flight constraint of constant bank angle (which replaces that of constant heading) and the two other constraints that define the preceding segment, which are maintained (for example, constant altitude and constant Mach).

The turn must be initiated some distance d before reaching the waypoint that triggers the heading change, see Fig. 6. This distance is calculated iteratively. To start the iteration, a first estimate is obtained considering uniform horizontal turns, in which case it is given by

$$d = R \tan\frac{\chi_{A_2} - \chi_{A_1}}{2} \tag{22}$$

where χ_{A_1} and χ_{A_2} are the old and new heading angles, and R is the turn radius which is given by

$$R = \frac{V^2}{g \tan\mu_A} \tag{23}$$

where V is approximated by $V \approx V_i$, V_i being the initial value of V during the preceding segment, which is known.

The stopping condition for the preceding segment is reaching the horizontal distance $r_A - d$, where r_A is the horizontal distance between the beginning of the preceding segment and the next waypoint (WP1 in Fig. 6), which is known. The stopping condition for the turning segment is reaching the new heading χ_{A_2}.

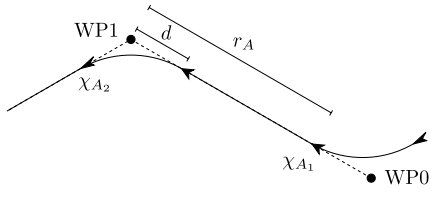

Fig. 6 Turn scheme.

4. Top of Descent

The top-of-descent (TOD) point is determined iteratively, to consider the actual weight of the aircraft (if the landing weight were known or guessed, the TOD point could be determined integrating backward, as in [29]).

As mentioned in Sec. II.A, we have defined the cruise speed reduction (CSR) point as the beginning of the last segment of the cruise phase. This segment is a deceleration at cruise altitude, that ends when the descent Mach number is reached. In the iteration procedure, the CSR point (instead of the TOD point) is determined iteratively, and, then, the TOD point is just the end of the segment; in this process, the trajectory is computed for different approximations of the CSR point until the touch down point coincides with the runway location.

IV. Scenarios

In this paper two scenarios are analyzed, one without locked aircraft and another with locked aircraft. In both cases the same TMA is considered: MADRID-BARAJAS airport (LEMD), RWY 18R, two TMA entry points (BARAHONA and TERSA) and one IAF (TAGOM).

In Scenario 1 the following traffic is considered:

1) Boeing 737/400, with TERSA as TMA entry point (labeled as A1 in the figures of Sec. V). The aircraft enters the scenario at $t = 0$ s, in cruise flight, at altitude $h_c = 30,000$ ft, and with mass $m = 50,631$ kg.

2) Airbus 320, with TERSA as TMA entry point (labeled as A2 in the figures of Sec. V). The aircraft enters the scenario at $t = 60$ s, in cruise flight, at altitude $h_c = 33,000$ ft, and with mass $m = 59,163$ kg.

3) Airbus 320, with BARAHONA as TMA entry point (labeled as A3 in the figures of Sec. V). The aircraft enters the scenario at $t = 300$ s, in descent flight, flying the constant-CAS segment, at an altitude $h_{\mathrm{TMA}} = 25,822$ ft, and with mass $m = 59,896$ kg.

4) CRJ 200, with BARAHONA as TMA entry point (labeled as A4 in the figures of Sec. V). The aircraft enters the scenario at $t = 360$ s, in descent flight, flying the constant-Mach segment, at an altitude $h_{\mathrm{TMA}} = 28,985$ ft, and with mass $m = 19,944$ kg.

In Scenario 2 the traffic considered has the same four unlocked aircraft of Scenario 1 plus the two following locked aircraft:

1) Boeing 737/400, with TERSA as TMA entry point (labeled as AL1 in the figures of Sec. V). The aircraft enters the scenario at $t = -60$ s, in cruise flight, at altitude $h_c = 30,000$ ft, and with mass $m = 50,631$ kg.

2) Airbus 320, with BARAHONA as TMA entry point (labeled as AL2 in the figures of Sec. V). The aircraft enters the scenario at $t = 120$ s, in descent flight, flying the constant-CAS segment, at an altitude $h_{\mathrm{TMA}} = 25,822$ ft, and with mass $m = 59,896$ kg.

The presence of the locked aircraft makes this scenario more exigent than Scenario 1 (although the parameters are the same, the number of constraints is larger). Hence, a higher cost of the resolution process is expected.

In these scenarios the same separation minima are considered for all pairs of aircraft, namely, $d_s = 3$ nmi and $h_s = 1000$ ft, and the conflict detection time step is $\Delta t = 0.1$ s. All turns are performed with bank angle $\mu_A = 25°$. The operational speeds are taken from BADA 3.6.

V. Results

Results are presented first for Scenario 1 (without locked aircraft) and then for Scenario 2 (with locked aircraft). In the following graphs, runways are represented by thick lines, VORs are circles, fix points are triangles, nominal waypoints are pentagrams, and aircraft are stars. Each aircraft is bounded by a cylinder of radius $d_s/2$ and height h_s; hence, when two cylinders intersect the distance between the aircraft is less than the separation minima (d_s and h_s) and a conflict exists.

In the results presented below, two types of conflict arise: *merging* and *catching up* (other types of conflicts are defined in [9]).

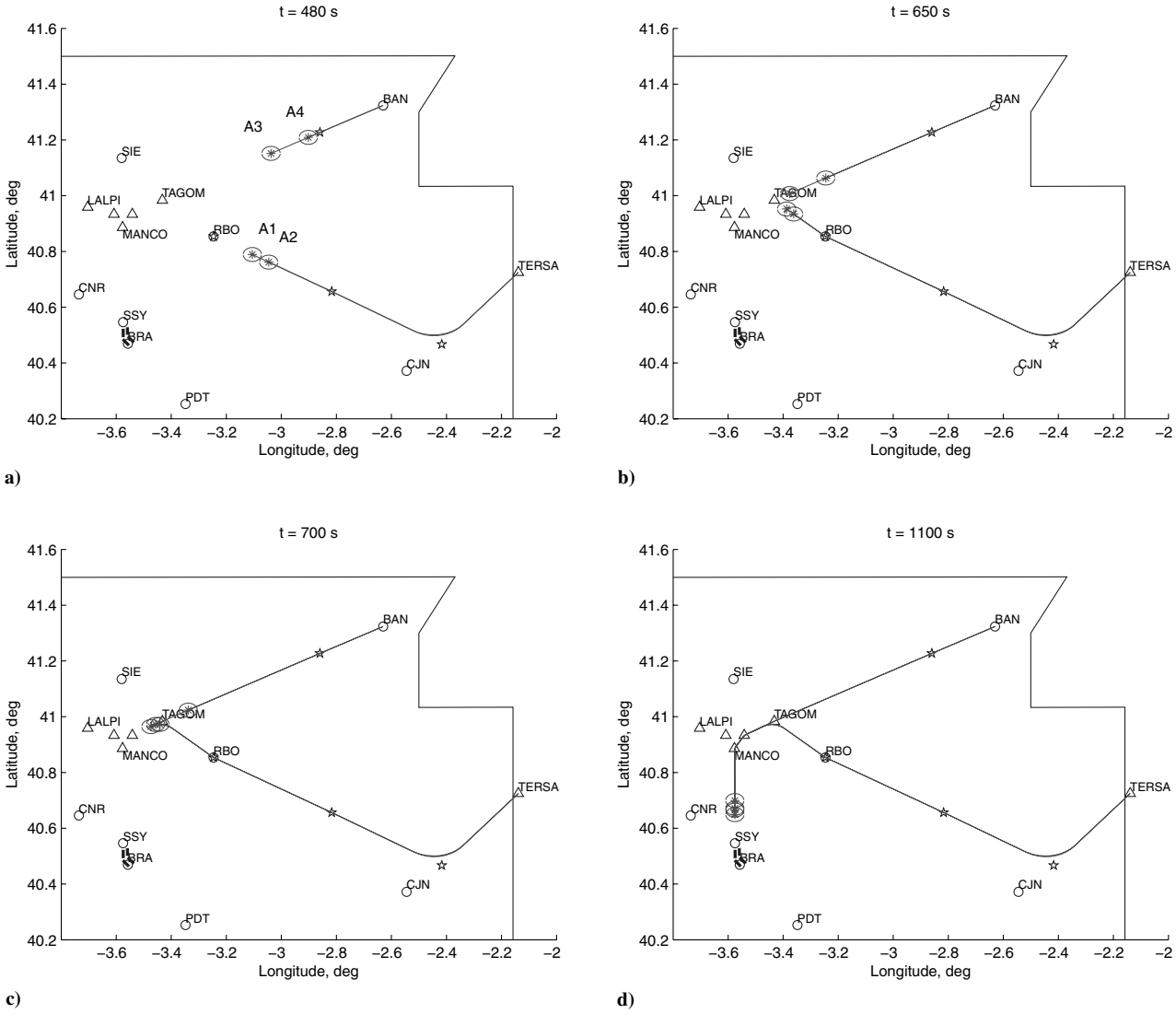

Fig. 7 Nominal trajectories without locked aircraft, at different times: a) 480 s, b) 650 s, c) 700 s, and d) 1100 s.

A. Scenario 1

1. Nominal Trajectories

The nominal trajectories are depicted at different times in Fig. 7. In Fig. 7a (at 480 s) all aircraft have entered the TMA and there is a catching-up conflict between aircraft A1 and A2; in Fig. 7b (at 650 s) a merging conflict between A1 and A3 arises; in Fig. 7c (at 700 s) one has multiple mergings; and in Fig. 7d (at 1100 s) one has multiple catching ups. Even though the aircraft are in conflict during the final

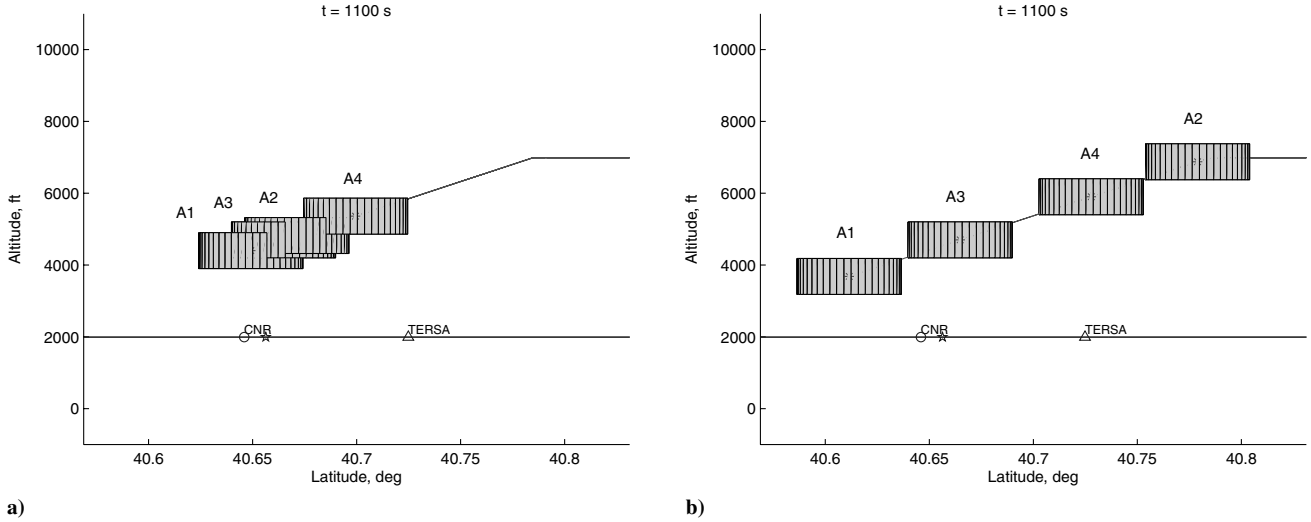

Fig. 8 Scenario 1: vertical profiles during the final approach: a) nominal trajectories, and b) resolution trajectories after phase 2.

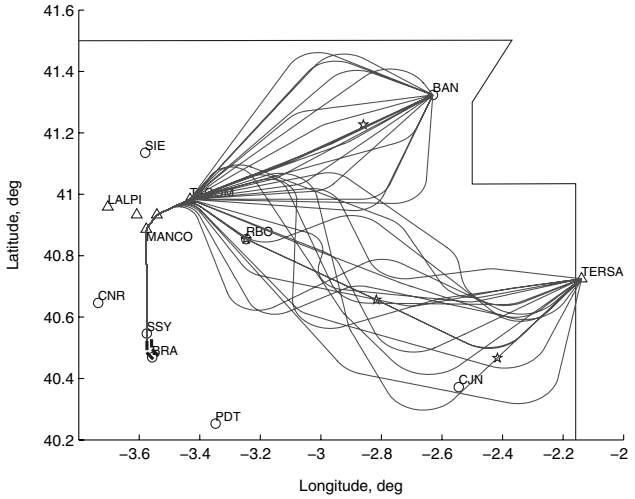

Fig. 9 Scenario 1: proposed trajectories in phase 1.

approach, the landing sequence for these nominal trajectories is A1-A3-A2-A4. Note that all those conflicts do exist, even though in Fig. 7 we only see the horizontal loss of separation (this same comment applies below, except in one case, stated explicitly, in which there is a horizontal loss of separation but there is not a conflict).

For aircraft A1 and A2, there are three waypoints that can be changed to resolve the conflicts, and for aircraft A3 and A4 there is only one. For A1 and A2, M_c, M_d, and CAS_d can be changed (since they enter the TMA in cruise flight); for A3 no speed can be changed (since it enters the TMA flying the constant-CAS segment); and for A4 only CAS_d can be modified (since it enters the TMA flying the constant-Mach segment).

The vertical profiles during the final approach (at 1100 s) are depicted in Fig. 8a, in which the multiple conflicts are clearly seen (for comparison, the vertical profiles for the resolution, conflict-free trajectories are also shown; they are analyzed below).

2. *Resolution Trajectories*

In the execution of the first phase of the resolution strategy, nine iterations were performed, hence nine trajectories were randomly generated for each aircraft. These trajectories and the nominal ones are shown in Fig. 9. In the last iteration of this first phase, 34 combinations of trajectories (out of a total of 10,000) met all the constraints. The lowest-cost combination, depicted in Fig. 10 at different times, was chosen as first valid solution; the cost of this solution is $f = 0.625$ (measured in degrees). The landing sequence in this solution is A1-A3-A4-A2.

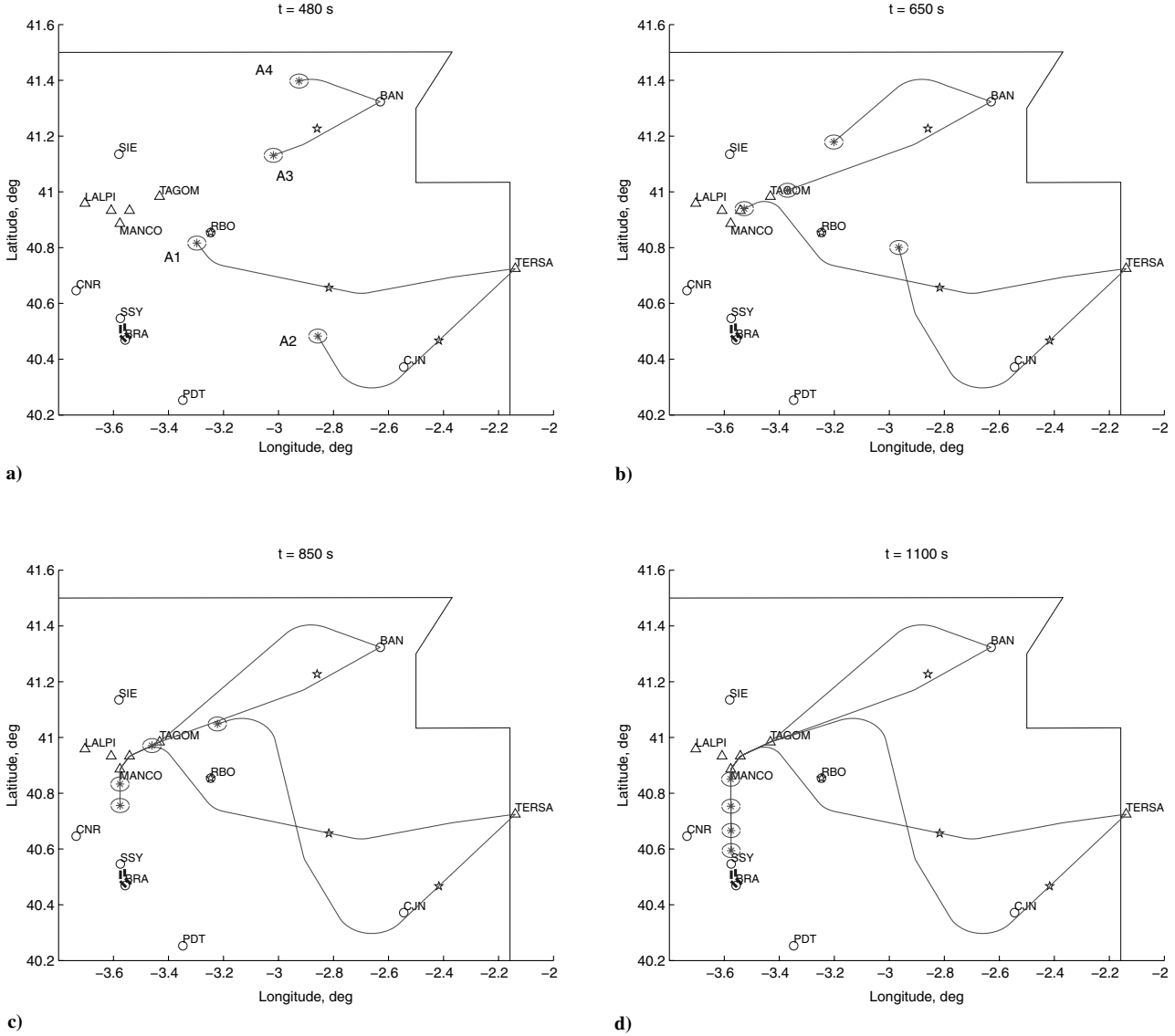

Fig. 10 Scenario1: resolution trajectories after phase 1 without locked aircraft, at different times: a) 480 s, b) 650 s, c) 850 s, and d) 1100 s.

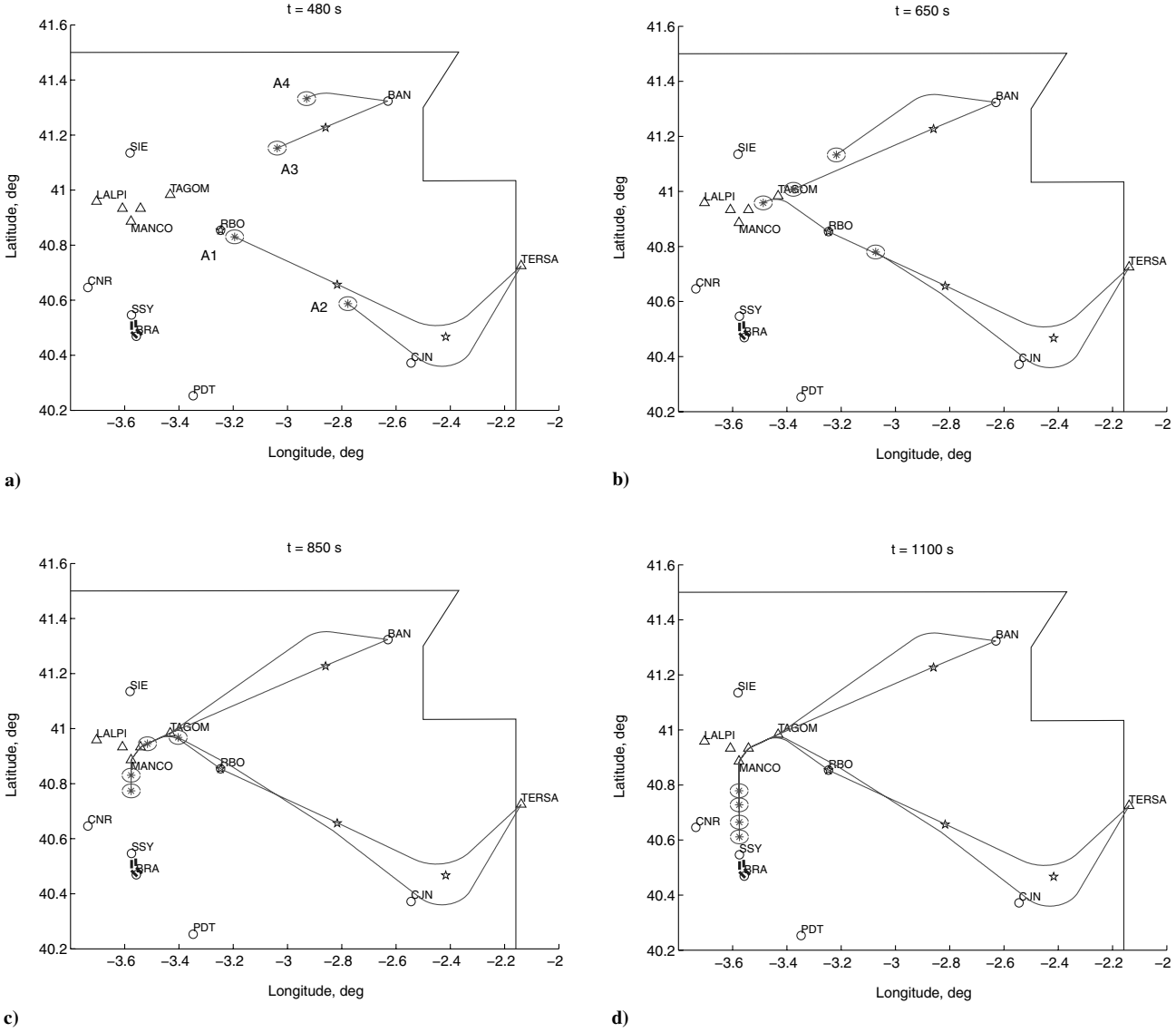

Fig. 11 Scenario 1: resolution trajectories after phase 2 without locked aircraft, at different times: a) 480 s, b) 650 s, c) 850 s, and d) 1100 s.

The resolution trajectories obtained after the second phase of the resolution strategy are depicted at different times in Fig. 11. In Fig. 11a (at 480 s) A2 and A4 are deviated; in Fig. 11b (at 650 s) A1 has crossed the IAF (TAGOM); in Fig. 11c (at 850 s) A3 and A4 have crossed the IAF and the landing sequence can be seen; and in Fig. 11d (at 1100 s) all aircraft are in the final approach conflict free. The landing sequence obtained in the resolution process is A1-A3-A4-A2 (the same as in the first phase). Note that A3 has followed very closely its nominal trajectory. The cost of this solution is $f = 0.223$. The vertical profiles during the final approach of these conflict-free resolution trajectories (at 1100 s) were depicted above in Fig. 8b.

With respect to the resolution strategy, the cost reduction (from 0.625 obtained in the first phase to 0.223) indicates the improvement obtained with the second phase.

The speed variations corresponding to these resolution trajectories are presented in Table 1 (along with the nominal values). A1 (that arrives in first place) has increased its speeds, whereas A2 and A4 have decreased theirs (to arrive later). Note that some speed changes have been the maximum 10% (recall that the cost function selected does not penalize speed variations).

Some global properties of the resolution trajectories are also presented in Table 1, namely, the increments in distance traveled Δr, flight time Δt_f, and fuel consumption Δm_F, between resolution and nominal trajectories. These increments are almost nil for A3, since it has followed its nominal trajectory. A1 has shortened its route slightly, decreasing the flight time, whereas A2 and A4 have lengthened theirs, increasing the flight time; Δr and Δt_f vary according to the landing sequence.

The total increase in fuel consumption is about 54 kg, which is a measure of the cost of the resolution process. Another performance indicator is the final value of the objective function, namely, $f = 0.223$.

Table 1 Scenario 1: properties of the resolution trajectories

Aircraft	M_c	ΔM_c	M_d	ΔM_d	CAS_d, kt	ΔCAS_d, kt	Δr, m	Δt_f, s	Δm_F, kg
A1	0.740	0.074	0.740	0.024	280.0	28.0	−1230	−59.0	27.3
A2	0.780	−0.078	0.780	−0.078	310.0	−31.0	23038	172.4	20.0
A3	——	——	——	——	310.0	——	3	0.0	0.0
A4	——	——	0.740	——	290.0	−4.1	5936	42.1	6.8

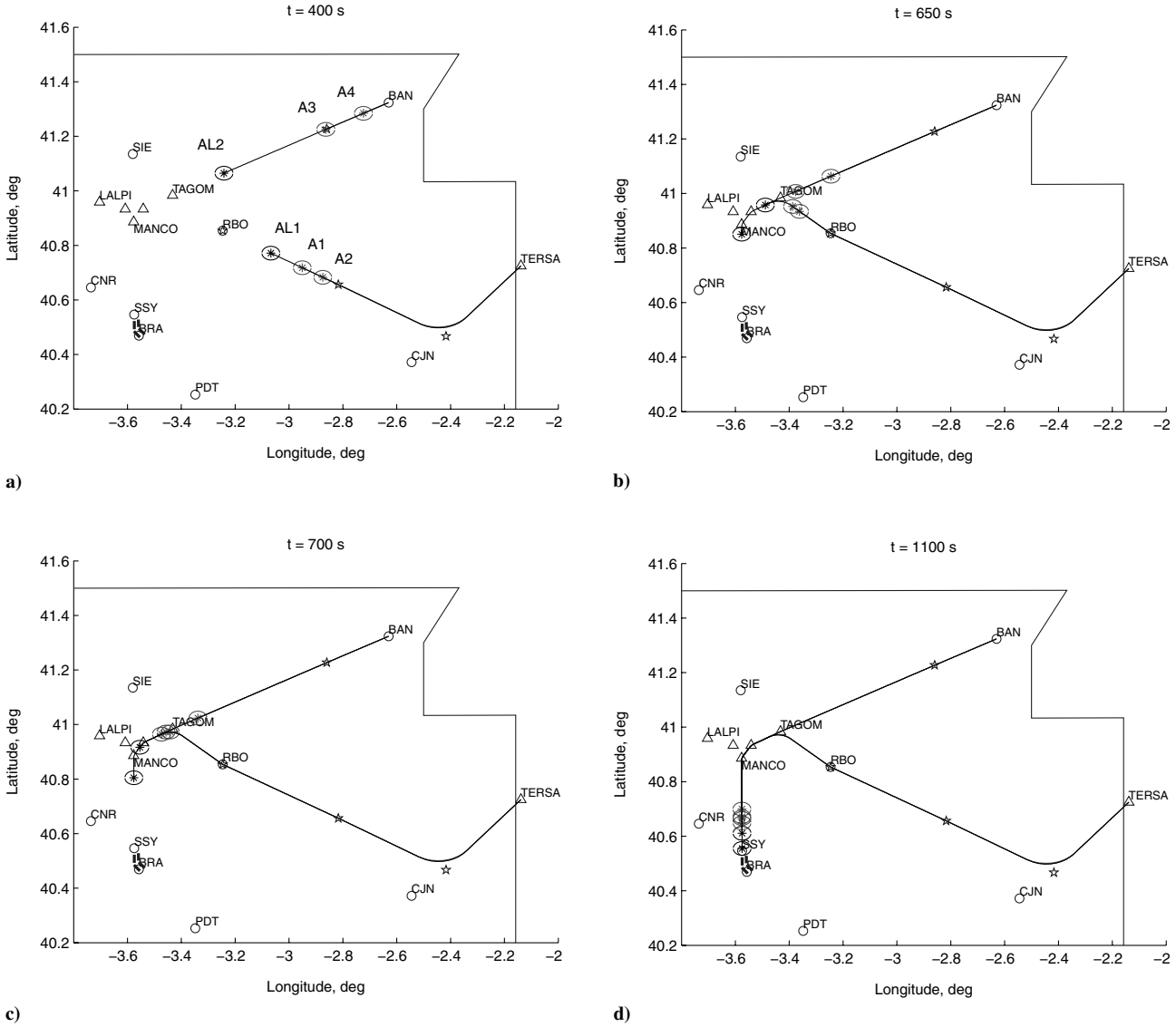

Fig. 12 Nominal trajectories with locked aircraft, at different times: a) 400 s, b) 650 s, c) 700 s, and d) 1100 s.

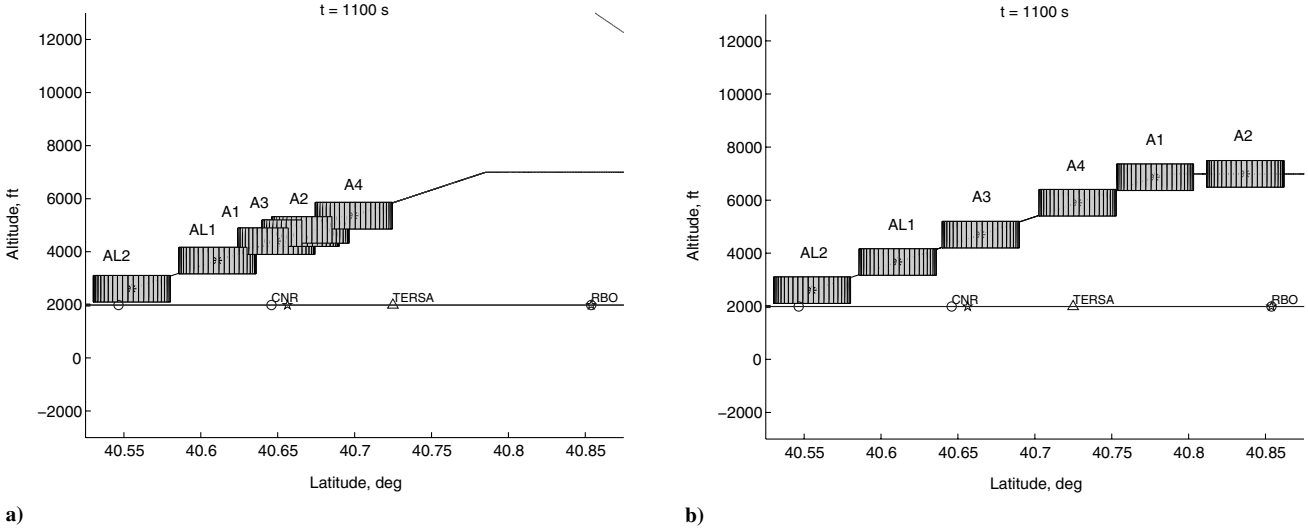

Fig. 13 Scenario 2: vertical profiles during the final approach: a) nominal trajectories, and b) resolution trajectories after phase 2.

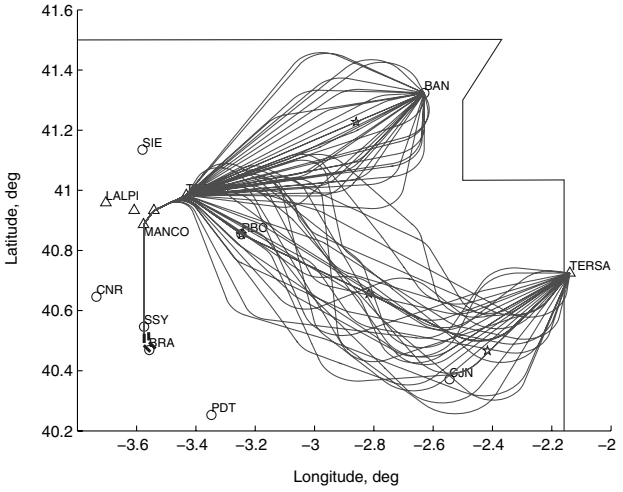

Fig. 14 Scenario 2: proposed trajectories in phase 1.

B. Scenario 2

1. Nominal Trajectories

The nominal trajectories in this second scenario are depicted at different times in Fig. 12. The trajectories of the two locked aircraft are such that there are no conflicts between them, but there exists a catching up between AL1 and A1 (see Fig. 12d). The landing sequence for these nominal trajectories is AL2-AL1-A1-A3-A2-A4.

As in Scenario 1, for aircraft A1 and A2 there are three waypoints that can be changed to resolve the conflicts, and for aircraft A3 and A4 there is only one. For A1 and A2, M_c, M_d, and CAS_d can be changed; for A3 no speed can be changed; and for A4 only CAS_d can be modified.

The vertical profiles during the final approach (at 1100 s) are depicted in Fig. 13a, in which the multiple conflicts among unlocked aircraft, as well as the catching up between A1 and AL1, are seen (for comparison, the vertical profiles for the resolution trajectories, which are analyzed below, are also shown; all the aircraft are there free of conflicts).

2. Resolution Trajectories

In the execution of the first phase in this second scenario 16 iterations were performed, hence 16 trajectories were randomly generated for each aircraft. Because of the higher exigency of this scenario, more iterations are performed than in Scenario 1. In the last iteration of this first phase, 17 combinations of trajectories (out of a total of 83521) met all the constraints. The generated trajectories and the nominal ones are shown in Fig. 14; since the changes in the waypoints coordinates are constrained to be enclosed inside given boxes, the proposed trajectories are contained in a sort of bands around the nominal trajectories, which can be seen in the figure. The

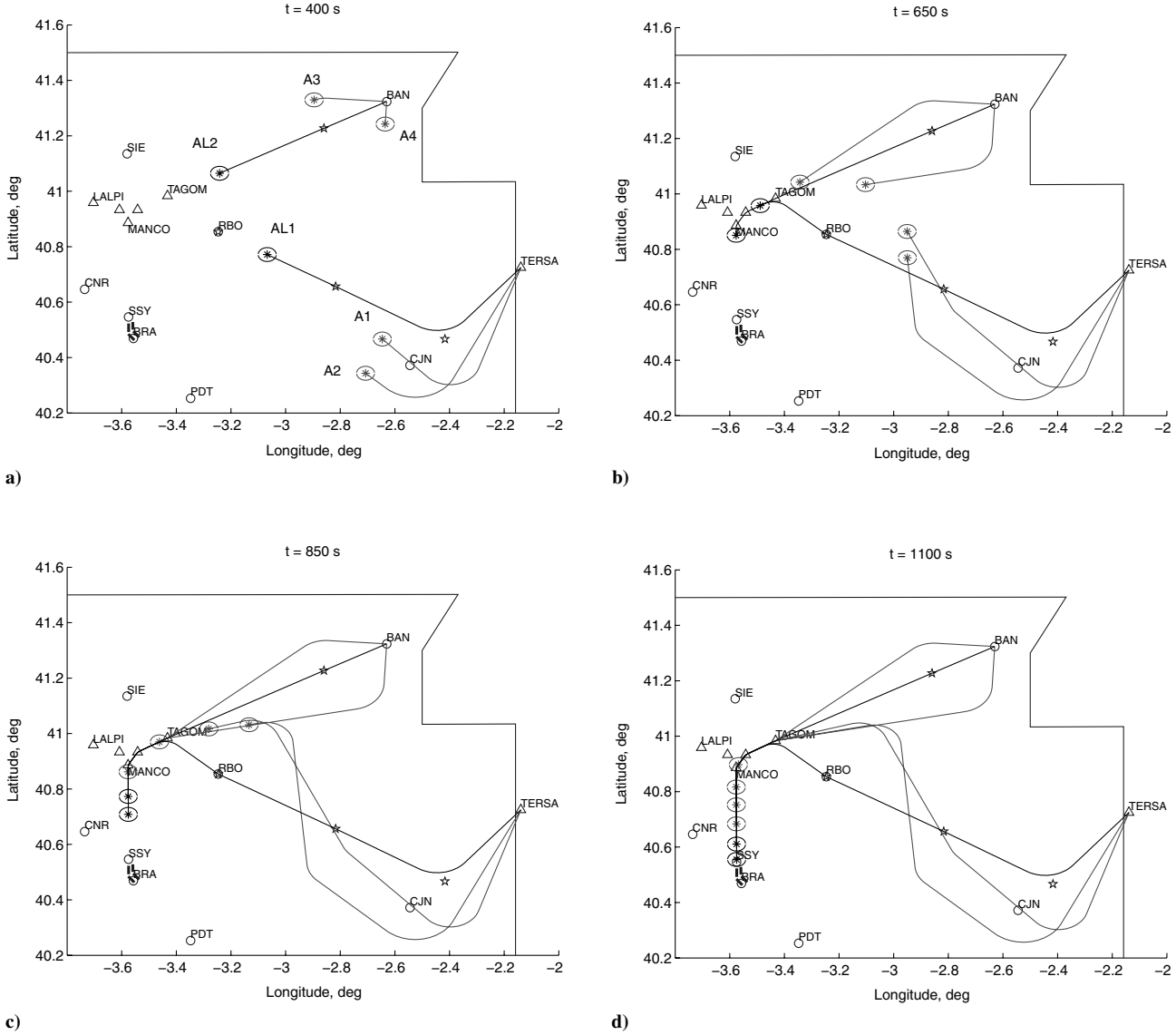

Fig. 15 Scenario 2: resolution trajectories after phase 1 with locked aircraft, at different times: a) 400 s, b) 650 s, c) 850 s, and d) 1100 s.

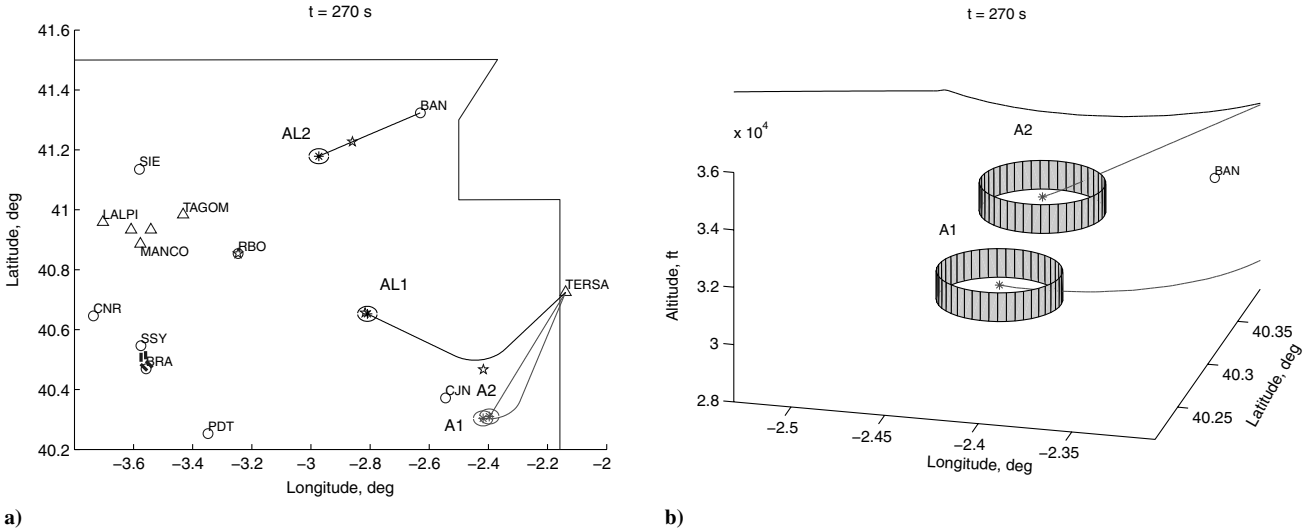

a) b)

Fig. 16 Scenario 2: resolution trajectories after phase 1 with locked aircraft, at 270 s: a) horizontal profile, and b) three-dimensional view.

lowest-cost combination, depicted in Fig. 15 at different times, was chosen as first valid solution. The cost of this solution is $f = 0.675$ (measured in degrees). The landing sequence in this solution is AL2-AL1-A3-A4-A1-A2.

In Fig. 16 we represent the resolution trajectories after phase 1 at 270 s. In this figure we can see a case in which the horizontal separation minimum is violated (the horizontal distance between A1 and A2 is smaller than d_s), but the vertical separation minimum is not

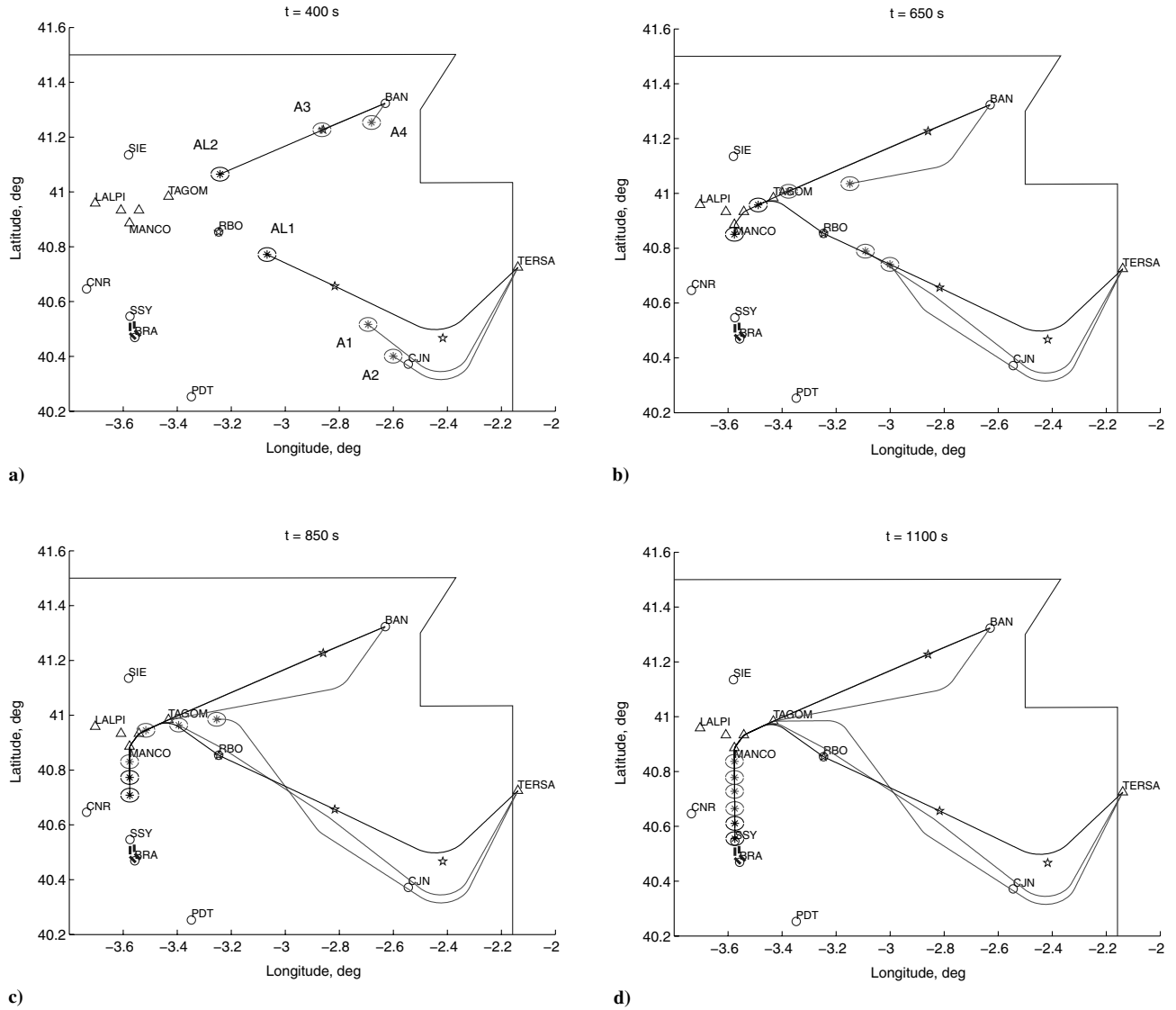

a) b) c) d)

Fig. 17 Scenario 2: resolution trajectories after phase 2 with locked aircraft, at different times: a) 400 s, b) 650 s, c) 850 s, and d) 1100 s.

Table 2 Scenario 2: properties of the resolution trajectories

Aircraft	M_c	ΔM_c	M_d	ΔM_d	CAS_d, kt	$\Delta\mathrm{CAS}_d$, kt	Δr, m	Δt_f, s	Δm_F, kg
A1	0.740	−0.074	0.740	−0.074	280.0	−28.0	25526	197.8	43.1
A2	0.780	−0.078	0.780	−0.078	310.0	−31.0	38845	247.9	63.9
A3	——	——	——	——	310.0	——	3	0.0	0.0
A4	——	——	0.740	——	290.0	−4.1	5948	42.1	6.8

(the vertical separation distance is larger than h_s), so that there is not a conflict.

The resolution trajectories obtained after the second phase are depicted at different times in Fig. 17. In Fig. 17a (at 400 s) A1, A2, and A4 are deviated; in Fig. 17b (at 650 s) A3 is reaching the IAF; in Fig. 17c (at 850 s) A4 has crossed the IAF; and in Fig. 17d (at 1100 s) all aircraft are in the final approach conflict free. Note that A3 has followed very closely its nominal trajectory. The landing sequence obtained in the resolution process is AL2-AL1-A3-A4-A1-A2 (the same as in the first phase). In this scenario the landing sequence of the unlocked aircraft is different from the sequence in Scenario 1. The cost of this solution is $f = 0.365$. The vertical profiles during the final approach of these conflict-free resolution trajectories (at 1100 s) were depicted in Fig. 13b.

Again, the cost reduction (from 0.675 to 0.365) indicates the improvement obtained with the second phase of the resolution strategy.

The speed variations and the global properties corresponding to these resolution trajectories are presented in Table 2. Except for $\Delta\mathrm{CAS}_d$ for A4, all speed changes have been maximum (10%), and in all cases the speeds have decreased.

The global properties indicate that A3 has followed almost exactly its nominal trajectory, whereas A1, A2, and A4 have lengthened their routes, increasing the flight time; Δr and Δt_f vary according to the landing sequence.

The total increase in fuel consumption is about 114 kg, significantly greater than in Scenario 1, as well as the final value of the objective function ($f = 0.365$), as expected for this more demanding scenario.

VI. Conclusions

In this paper a method for conflict detection and resolution in converging traffic in the terminal area has been presented. The conflict detection and resolution algorithms rely on a kinetic-based trajectory predictor that is accurate, flexible, and transparent, and provides the high-fidelity prediction that is required in the demanding terminal area traffic management.

The method is based on the parameterization of the aircraft intents. To perform this parameterization, predefined trajectory patterns have been considered. The resolution trajectory patterns take into account changes of the nominal waypoints (vectoring) and changes of the aircraft speeds. The conflict resolution problem has been formulated as a parametric optimization problem subject to constraints. The method has been applied to the case of global traffic (multiple conflicts) in two different scenarios: one with only unlocked aircraft, and another one with some additional locked aircraft. The two-phase resolution strategy considered has proven to be an efficient approach, both in finding a first valid solution with a relatively small number of trajectory computations, and improving it by reducing the total cost. The cost of the resolution process has been assessed in terms of extra distance traveled, extra flight time, and extra fuel consumption for each aircraft. As expected, the scenario with additional locked aircraft has been more demanding in computing effort, and the cost of the resolution process has been larger.

This method can be generalized straightforwardly to solve other problems, for example, to account for constraints imposed by the existence of restricted areas (of known geometry); or to consider additional constraints as in the meet-time problem (sequencing and scheduling). The method can be also applied to other types of traffic, for example, enroute traffic (free flight), and can incorporate other features such as altitude changes, which would just require the definition of the appropriate trajectory patterns. Likewise, the trajectory computation solver can be extended to consider other flight segments that might be required (for instance, CAS/Mach climb with maximum climb engine rating).

As already mentioned, the conflict detection and resolution algorithm is global, meaning that all the aircraft present in the scenario are handled altogether, which in fact limits the number of aircraft that can be handled, especially in the second phase of the resolution strategy (optimization) since the number of parameters can become excessively large. However, in practice, the landing sequence is known, in which case the aircraft can be processed sequentially (aircraft i only interacts with aircraft $1, 2 \ldots i-1$); this real case is less demanding than the global case considered in the paper, and, in fact, preliminary results show that up to 35 aircraft arriving in 1 h can be analyzed. The analysis of this problem is left for future work.

Appendix A: Trajectory Computation Solver

The trajectory computation solver computes each flight segment, which requires solving the corresponding DAE system. In the solver presented in this paper, the control variables (T, L, μ) are determined explicitly (operation that can be accomplished in all the flight segments considered) and the DAE system is reduced to an ODE system, that can be solved using standard numerical procedures, such as a Runge–Kutta method. In the following, each type of flight segment is described, and the corresponding equations of motion [ODE system to be solved, obtained from Eqs. (17)] are summarized.

I. Horizontal, Rectilinear, Uniform Flight

Constraints: 1) constant altitude $h = h_A$, 2) constant Mach or constant CAS, that is, known speed law $V = V_M(h)$ or $V = V_C(h)$, respectively, that is, known speed law $V = V(h)$, and 3) constant heading angle $\chi = \chi_A$.

In this segment, since $h = \text{const}$, one has $V = \text{const}$, say $V = V(h_A) \equiv V_A$; one also has $L = mg$, $\mu = 0$ and $\gamma = 0$. Equations (17) reduce to:

$$\begin{aligned} \frac{\mathrm{d}m}{\mathrm{d}t} &= -c(M_A, h_A)T(m) \\ (R_E + h_A)\frac{\mathrm{d}\varphi}{\mathrm{d}t} &= V_A \cos\chi_A \\ (R_E + h_A)\cos\varphi\frac{\mathrm{d}\lambda}{\mathrm{d}t} &= V_A \sin\chi_A \end{aligned} \tag{A1}$$

where the required thrust $T(m)$ is given by

$$T = \frac{1}{2}\rho_A V_A^2 S C_D(M_A, C_L) \tag{A2}$$

with

$$C_L = \frac{2mg}{\rho_A V_A^2 S} \tag{A3}$$

II. Horizontal Acceleration/Deceleration in Rectilinear Flight

Constraints: 1) constant altitude $h = h_A$, 2) given engine rating, either maximum cruise $T = T_{\mathrm{MCRZ}}(M, h)$ or idle $T = T_{\mathrm{IDLE}}(M, h)$, that is, a known function $T(M, h)$, and 3) constant heading angle $\chi = \chi_A$.

In this segment one has $L = mg$, $\mu = 0$ and $\gamma = 0$. The equations of motion (17) reduce to:

$$\begin{aligned} m\frac{\mathrm{d}V}{\mathrm{d}t} &= T(M, h_A) - \frac{1}{2}\rho_A V^2 S C_D(M, C_L) \\ \frac{\mathrm{d}m}{\mathrm{d}t} &= -c(M, h_A)T(M, h_A) \\ (R_E + h_A)\frac{\mathrm{d}\varphi}{\mathrm{d}t} &= V\cos\chi_A \\ (R_E + h_A)\cos\varphi\frac{\mathrm{d}\lambda}{\mathrm{d}t} &= V\sin\chi_A \end{aligned} \tag{A4}$$

where the lift coefficient $C_L(V, m)$ is given by

$$C_L = \frac{2mg}{\rho_A V^2 S} \tag{A5}$$

III. Mach/CAS Descent in Rectilinear Flight

Constraints: 1) constant Mach or constant CAS, that is, known speed law $V = V_M(h)$ or $V = V_C(h)$, respectively, 2) idle engine rating $T = T_{\mathrm{IDLE}}(M, h)$, and 3) constant heading angle $\chi = \chi_A$.

In general, in this segment one has known functions $V(h)$ and $T(M, h)$; one also has $\mu = 0$. The equations of motion (17) reduce to:

$$\begin{aligned} mV(h)\frac{\mathrm{d}\gamma}{\mathrm{d}t} &= L(m, h, \gamma) - mg\cos\gamma \\ \frac{\mathrm{d}m}{\mathrm{d}t} &= -c(M, h)T(M, h) \\ (R_E + h)\frac{\mathrm{d}\varphi}{\mathrm{d}t} &= V(h)\cos\gamma\cos\chi_A \\ (R_E + h)\cos\varphi\frac{\mathrm{d}\lambda}{\mathrm{d}t} &= V(h)\cos\gamma\sin\chi_A \\ \frac{\mathrm{d}h}{\mathrm{d}t} &= V(h)\sin\gamma \end{aligned} \tag{A6}$$

where the lift $L(m, h, \gamma)$ is given by

$$L = \frac{1}{2}\rho V^2(h) S C_L(m, h, \gamma) \tag{A7}$$

and the lift coefficient $C_L(m, h, \gamma)$ is the solution of

$$\frac{1}{2}\rho V^2(h) S C_D(M, C_L) = T(M, h) - mg\sin\gamma - mV(h)\frac{\mathrm{d}V}{\mathrm{d}h}\sin\gamma \tag{A8}$$

IV. Glide Path

Constraints: 1) constant path angle $\gamma = \gamma_A$ (defined by the ILS), 2) constant CAS (in practice, the approach speed $\mathrm{CAS}_{\mathrm{AP}}$), that is, known speed law $V = V_C(h)$, and 3) constant heading angle $\chi = \chi_A$.

In this segment one has $L = mg\cos\gamma_A$ and $\mu = 0$. Equations (17) reduce to

$$\begin{aligned} \frac{\mathrm{d}m}{\mathrm{d}t} &= -c(M, h)T(h, m) \\ (R_E + h)\frac{\mathrm{d}\varphi}{\mathrm{d}t} &= V_C(h)\cos\gamma_A\cos\chi_A \\ (R_E + h)\cos\varphi\frac{\mathrm{d}\lambda}{\mathrm{d}t} &= V_C(h)\cos\gamma_A\sin\chi_A \\ \frac{\mathrm{d}h}{\mathrm{d}t} &= V_C(h)\sin\gamma_A \end{aligned} \tag{A9}$$

where the required thrust $T(h, m)$ is given by

$$T = \frac{1}{2}\rho V_C^2(h) S C_D(M, C_L) + mg\sin\gamma_A + mV_C(h)\frac{\mathrm{d}V_C}{\mathrm{d}h}\sin\gamma_A \tag{A10}$$

with

$$C_L = \frac{2mg\cos\gamma_A}{\rho V_C^2(h) S} \tag{A11}$$

V. Horizontal Turn in Uniform Flight

Constraints: 1) constant altitude $h = h_A$, 2) constant Mach or constant CAS, that is, known speed law $V = V_M(h)$ or $V = V_C(h)$, respectively, and 3) constant bank angle $\mu = \mu_A$.

In this segment, since $h = \mathrm{const}$, one has $V = \mathrm{const}$, say $V = V_A$; one also has $L = \frac{mg}{\cos\mu_A}$ and $\gamma = 0$. Equations (17) reduce to:

$$\begin{aligned} mV_A\frac{\mathrm{d}\chi}{\mathrm{d}t} &= L(m)\sin\mu_A \\ \frac{\mathrm{d}m}{\mathrm{d}t} &= -c(M_A, h_A)T(m) \\ (R_E + h_A)\frac{\mathrm{d}\varphi}{\mathrm{d}t} &= V_A\cos\chi \\ (R_E + h_A)\cos\varphi\frac{\mathrm{d}\lambda}{\mathrm{d}t} &= V_A\sin\chi \end{aligned} \tag{A12}$$

where the required thrust $T(m)$ is given by Eq. (A2), with the lift coefficient given by

$$C_L = \frac{2mg}{\rho_A V_A^2 S\cos\mu_A} \tag{A13}$$

VI. Horizontal Turn in Accelerating/Decelerating Flight

Constraints: 1) constant altitude $h = h_A$, 2) given engine rating, either maximum cruise $T = T_{\mathrm{MCRZ}}(M, h)$ or idle $T = T_{\mathrm{IDLE}}(M, h)$, that is, a known function $T(M, h)$, and 3) constant bank angle $\mu = \mu_A$.

In this segment one has $L = \frac{mg}{\cos\mu_A}$ and $\gamma = 0$. The equations of motion (17) reduce to:

$$\begin{aligned} m\frac{\mathrm{d}V}{\mathrm{d}t} &= T(M, h_A) - \frac{1}{2}\rho_A V^2 S C_D(M, C_L) \\ mV\frac{\mathrm{d}\chi}{\mathrm{d}t} &= L(m)\sin\mu_A \\ \frac{\mathrm{d}m}{\mathrm{d}t} &= -c(M, h_A)T(M, h_A) \\ (R_E + h_A)\frac{\mathrm{d}\varphi}{\mathrm{d}t} &= V\cos\chi \\ (R_E + h_A)\cos\varphi\frac{\mathrm{d}\lambda}{\mathrm{d}t} &= V\sin\chi \end{aligned} \tag{A14}$$

where the lift coefficient $C_L(V, m)$ is given by

$$C_L = \frac{2mg}{\rho_A V^2 S\cos\mu_A} \tag{A15}$$

VII. Turn in Mach/CAS Descent Flight

Constraints: 1) constant Mach or constant CAS, that is, known speed law $V = V_M(h)$ or $V = V_C(h)$, respectively, 2) idle engine rating $T = T_{\mathrm{IDLE}}(M, h)$, and 3) constant bank angle $\mu = \mu_A$.

In general, in this segment one has known functions $V(h)$ and $T(M, h)$. The equations of motion (17) reduce to

$$
\begin{aligned}
mV(h)\cos\gamma\frac{\mathrm{d}\chi}{\mathrm{d}t} &= L(m,h,\gamma)\sin\mu_A \\
mV(h)\frac{\mathrm{d}\gamma}{\mathrm{d}t} &= L(m,h,\gamma)\cos\mu_A - mg\cos\gamma \\
\frac{\mathrm{d}m}{\mathrm{d}t} &= -c(M,h)T(M,h) \\
(R_E+h)\frac{\mathrm{d}\varphi}{\mathrm{d}t} &= V(h)\cos\gamma\cos\chi \\
(R_E+h)\cos\varphi\frac{\mathrm{d}\lambda}{\mathrm{d}t} &= V(h)\cos\gamma\sin\chi \\
\frac{\mathrm{d}h}{\mathrm{d}t} &= V(h)\sin\gamma
\end{aligned}
\tag{A16}
$$

where the lift $L(m,h,\gamma)$ is given by Eq. (A7) and the lift coefficient $C_L(m,h,\gamma)$ is defined by Eq. (A8).

Appendix B. Supplementary Models

I. Earth Model

The Earth model adopted has the following characteristics: 1) Earth radius $R_E = 6356.766$ km, 2) constant gravity $g = 9.80665\ \mathrm{m/s^2}$, 3) air, a perfect gas defined by a ratio of specific heats $\kappa = 1.4$ and a gas constant $R_a = 287.053\ \mathrm{J/(kg\,K)}$, and 4) standard atmosphere ISA (it defines temperature, Θ, pressure, p, and density, ρ, as functions of h).

II. Aerodynamic Model

The aerodynamic model defines the drag polar $C_D = C_D(M, C_L)$, that gives the drag coefficient as a function of Mach number M and lift coefficient C_L. The lift and drag coefficients are defined by $L = \frac{1}{2}\rho V^2 S C_L$ and $D = \frac{1}{2}\rho V^2 S C_D$, respectively. The drag polar must take into account the aerodynamic configuration (clean, high-lift devices, landing gear, spoilers).

In this paper the operational speeds and the drag polar coefficients used in the computations are taken from BADA 3.6.

III. Propulsion Model

The propulsion model defines the thrust available and the specific fuel consumption.

A. Thrust

For the available thrust the following general model is considered (see Torenbeek [30])

$$T = W_{\mathrm{TO}}\delta C_T(M, N_c) \tag{B1}$$

where W_{TO} is the reference takeoff weight, $\delta = p/p_{\mathrm{SL}}$ is the pressure ratio, and C_T is the thrust coefficient, which in general is a function of the Mach number and the engine control parameter N_c. For a given *engine rating* (maximum cruise or idle), the control parameter is a function of Mach number and altitude ($N_c(M,h)$), therefore one can also write the model as $T = T_{\mathrm{RATE}}(M,h)$, that is, thrust dependent both on Mach number and altitude.

Although different functional dependencies should be used for the various engine ratings, in this paper, for simplicity, the following single model is considered for the thrust coefficient (see Mattingly et al. [31] and Barman and Erzberger [32])

$$C_T = \frac{T_{\mathrm{SL,RATE}}}{W_{\mathrm{TO}}}\left(1+\frac{\kappa-1}{2}M^2\right)^{\frac{\kappa}{\kappa-1}}(1-0.49\sqrt{M})\frac{1}{\theta} \tag{B2}$$

where $T_{\mathrm{SL,RATE}}$ is the thrust at sea level and for $M = 0$ for the given engine rating.

The values of $T_{\mathrm{SL,RATE}}$ used in the computations are taken from BADA 3.6.

B. Specific Fuel Consumption

For the specific fuel consumption the following general model is considered (see Torenbeek [30])

$$c = \frac{a_{\mathrm{SL}}\sqrt{\theta}}{L_H}C_C(M) \tag{B3}$$

where $a_{\mathrm{SL}} = \sqrt{\kappa R_a \Theta_{\mathrm{SL}}}$ is the speed of sound at sea level, $\theta = \Theta/\Theta_{\mathrm{SL}}$ is the temperature ratio, L_H is the fuel latent heat, and C_C is the specific fuel consumption coefficient (in general C_C depends on C_T, but this dependence is neglected, since it is very weak in practice [30]).

For the specific fuel consumption coefficient, the linear model defined by Mattingly et al. [31] is considered; it is given by

$$C_C = c_{\mathrm{SL}}\frac{L_H}{a_{\mathrm{SL}}}(1.0 + 1.2M) \tag{B4}$$

where c_{SL} is the specific fuel consumption at sea level and for $M = 0$. For the fuel latent heat, one can take $L_H = 43 \times 10^6\ \mathrm{J/kg}$.

The values of c_{SL} used in the computations are taken from BADA 3.6.

References

[1] Menon, P. K., Sweriduk, G. D., and Sridhar, B., "Optimal Strategies for Free-Flight Air Traffic Conflict Resolution," *Journal of Guidance, Control, and Dynamics*, Vol. 22, No. 2, 1999, pp. 202–211. doi:10.2514/2.4384

[2] Frazzoli, E., Mao, Z.-H., Oh, J.-H., and Feron, E., "Resolution of Conflicts Involving Many Aircraft via Semidefinite Programming," *Journal of Guidance, Control, and Dynamics*, Vol. 24, No. 1, 2001, pp. 79–86. doi:10.2514/2.4678

[3] Hu, J., Prandini, M., and Sastry, S., "Optimal Coordinated Maneuvers for Three-Dimensional Aircraft Conflict Resolution," *Journal of Guidance, Control, and Dynamics*, Vol. 25, No. 5, 2002, pp. 888–900. doi:10.2514/2.4982

[4] Clements, J. C., "Optimal Simultaneous Pairwise Conflict Resolution Maneuvers in Air Traffic Management," *Journal of Guidance, Control, and Dynamics*, Vol. 25, No. 4, 2002, pp. 815–818. doi:10.2514/2.4950

[5] Paielli, R. A., "Modeling Maneuver Dynamics in Air Traffic Conflict Resolution," *Journal of Guidance, Control, and Dynamics*, Vol. 26, No. 3, 2003, pp. 407–415. doi:10.2514/2.5078

[6] Raghunathan, A. U., Gopal, V., and Subramanian, D., "Dynamic Optimization Strategies for Three-Dimensional Conflict Resolution of Multiple Aircraft," *Journal of Guidance, Control, and Dynamics*, Vol. 27, No. 4, 2004, pp. 586–594. doi:10.2514/1.11168

[7] Vivona, R. A., Karr, D. A., and Roscoe, D. A., "Pattern-Based Genetic Algorithm for Airborne Conflict Resolution," AIAA Paper 2006-6060, 2006.

[8] Bilimoria, K. D., and Lee, H. Q., "Aircraft Conflict Resolution with an Arrival Time Constraint," AIAA Paper 2002-4444, 2002.

[9] Isaacson, D. R., and Robinson J. E. III., "A Knowledge-Based Conflict Resolution Algorithm for Terminal Area Air Traffic Control Advisory Generation," AIAA Paper 2001-4116, 2001.

[10] Kuchar, J. K., and Yang, L. C., "A Review of Conflict Detection and Resolution Modeling Methods," *IEEE Transactions on Intelligent Transportation Systems*, Vol. 1, No. 4, 2000, pp. 179–189. doi:10.1109/6979.898217

[11] Vilaplana, M. A., "Co-operative Conflict Resolution in Autonomous Aircrfat Operations Using a Multi-Agent Approach," Ph.D. Thesis, Univ. of Glasgow, 2002.

[12] Coppenbarger, R. A., Lanier, R., Sweet, D., and Dorsky, S., "Design and Development of the En Route Descent Advisor (EDA) for Conflict-Free Arrival Metering," AIAA Paper 2004-4875, 2004.

[13] Gill, W., and Maddock, R., "EFMS Prediction of Optimal 4-D Trajectories in the presence of Time and Altitude Constraints," EUROCONTROL PHARE DOC 97-70-09, 1997.

[14] Slattery, R. A., and Zhao, Y., "Trajectory Synthesis for Air Traffic Automation," *Journal of Guidance, Control, and Dynamics*, Vol. 20, No. 2, 1997, pp. 232–238. doi:10.2514/2.4056

[15] Jackson, M. R., Zhao, Y., and Slattery, R. A., "Sensitivity of Trajectory

Prediction in Air Traffic Management," *Journal of Guidance, Control, and Dynamics*, Vol. 22, No. 2, 1999, pp. 219–228.
doi:10.2514/2.4398

[16] Barrer, J. N., "Integrating the Flight Management System with Air Traffic Control Functions: The Concept of Path Objects," MITRE Corporation Technical Rept. MTR 99W000011, 1999.

[17] Bilimoria, K. D., "A Geometric Optimization Approach to Aircraft Conflict Resolution," AIAA Paper 2000-4265, 2000.

[18] Valenzuela, A., and Rivas, D., "Conflict Detection and Resolution in Converging Air Traffic," AIAA Paper 2009-7022, 2009.

[19] Bilimoria, K. D., Sheth, K. S., Lee, H. Q., and Grabbe, S. R., "Performance Evaluation of Airborne Separation Assurance for Free Flight," AIAA Paper 2000-4269, 2000.

[20] Dowek, G., and Muñoz, C., Conflict Detection and Resolution for $1, 2, \ldots N$ Aircraft, AIAA Paper 2007-7737, 2007.

[21] Isaacson, D. R., and Erzberger, H., "Design of a Conflict Detection Algorithm for the Center/TRACON Automation System," *Proceedings 16th Digital Avionics Systems Conference*, IEEE Publications, Piscataway, NJ, Oct. 1997, pp. 1–9.

[22] Kremer, H. J., Vertegaal, W. C., and Jansen, R. B. H. J., "PHARE Advanced Tools: Conflict Probe," EUROCONTROL, PHARE DOC 98-70-18, Vol. 3, 1999.

[23] Rao, S. S., *Engineering Optimization. Theory and Practice*, 3rd ed., Wiley, New York, 1996, pp. 491–492.

[24] Gill, P. E., Murray, W., Saunders, M. A., and Wright, M. H., "Constrained Nonlinear Programming," *Handbooks in Operations Research and Management Science*, Vol. 1, edited by G. L. Nemhauser, A. H. G. Rinnooy Kan, and M. J. Todd, Elsevier Science, Amsterdam, 1989, pp 193–200.

[25] Fletcher, R., *Practical Methods of Optimization*, John Wiley & Sons Ltd., New York, 1987, p. 71.

[26] Base of Aircraft Data (BADA): Revision 3.6, EUROCONTROL, 2004.

[27] López, J., Vilaplana, M. A., Gallo, E., Navarro, F. A., and Querejeta, C., "The Aircraft Intent Description Language: A Key Enabler for Air-Ground Synchronization in Trajectory-Based Operations," *Proceedings 26th Digital Avionics Systems Conference*, IEEE Publications, Piscataway, NJ, Oct. 2007, pp. 1–12.

[28] Asselin, M., *An Introduction to Aircraft Performance*, AIAA Education Series, AIAA, Reston, VA, 1997, p. 323.

[29] Williams, D. H., and Green, S. M., "Airborne Four-Dimensional Flight Management in a Time-Based Air Traffic Control Environment," NASA TM-4249, 1991.

[30] Torenbeek, E., "Cruise Performance and Range Prediction Reconsidered," *Progress in Aerospace Sciences*, Vol. 33, Nos. 5–6, 1997, pp. 285–321.
doi:10.1016/S0376-0421(96)00007-3

[31] Mattingly, J. D., Heiser, W. H., and Pratt, D. T., *Aircraft Engine Design*, 2nd ed., AIAA Education Series, AIAA, Reston, VA, 2002, pp. 38, 71.

[32] Barman, J. F., and Erzberger, H., "Fixed-Range Optimum Trajectories for Short-Haul Aircraft," *Journal of Aircraft*, Vol. 13, No. 10, 1976, pp. 748–754.
doi:10.2514/3.58706